HAL
open science

A SOPHIE RV search for giant planets around young nearby stars (YNS)

A. Grandjean, A.-M. Lagrange, N. Meunier, P. Rubini, S. Desidera, F. Galland, S. Borgniet, N. Zicher, S. Messina, G. Chauvin, et al.

To cite this version:

A. Grandjean, A.-M. Lagrange, N. Meunier, P. Rubini, S. Desidera, et al.. A SOPHIE RV search for giant planets around young nearby stars (YNS). Astronomy and Astrophysics - A&A, 2021, 650, pp.A39. 10.1051/0004-6361/202039672 . hal-03278075

HAL Id: hal-03278075

https://hal.sorbonne-universite.fr/hal-03278075v1

Submitted on 5 Jul 2021

HAL is a multi-disciplinary open access archive for the deposit and dissemination of scientific research documents, whether they are published or not. The documents may come from teaching and research institutions in France or abroad, or from public or private research centers.

L'archive ouverte pluridisciplinaire **HAL**, est destinée au dépôt et à la diffusion de documents scientifiques de niveau recherche, publiés ou non, émanant des établissements d'enseignement et de recherche français ou étrangers, des laboratoires publics ou privés.

A&A 650, A39 (2021)
https://doi.org/10.1051/0004-6361/202039672
© A. Grandjean et al. 2021

Astronomy & Astrophysics

A SOPHIE RV search for giant planets around young nearby stars (YNS)

A combination with the HARPS YNS survey*

A. Grandjean[1], A.-M. Lagrange[1,2,3], N. Meunier[1], P. Rubini[4], S. Desidera[5], F. Galland[1], S. Borgniet[6], N. Zicher[7], S. Messina[8], G. Chauvin[1], M. Sterzik[9], and B. Pantoja[10]

[1] Univ. Grenoble Alpes, CNRS, IPAG, 38000 Grenoble, France
e-mail: antoine.grandjean1@univ-grenoble-alpes.fr
[2] LESIA, Observatoire de Paris, Université PSL, CNRS, Sorbonne Université, Université de Paris, 5 place Jules Janssen, 92195 Meudon, France
[3] IMCCE – Observatoire de Paris, 77 Avenue Denfert-Rochereau, 75014 Paris, France
[4] Pixyl, 5 Avenue du Grand Sablon, 38700 La Tronche, France
[5] INAF-Osservatorio Astronomico di Padova, Vicolo dell'Osservatorio 5, 35122 Padova, Italy
[6] CNRS Lesia (UMR8109) – Observatoire de Paris, Paris, France
[7] Oxford Astrophysics, Department of Physics, Denys Wilkinson Building, UK
[8] INAF-Osservatorio Astrofisico di Catania, via Santa Sofia, 78 Catania, Italy
[9] European Southern Observatory, Karl-Schwarzschild-Str 1, 85748 Garching, Germany
[10] Departamento de Astronomía, Universidad de Chile, Camino al Observatorio, Cerro Calán, Santiago, Chile

Received 13 October 2020 / Accepted 26 February 2021

ABSTRACT

Context. The search of close ($a \lesssim 5$ au) giant planet (GP) companions with radial velocity (RV) around young stars and the estimate of their occurrence rates is important to constrain the migration timescales. Furthermore, this search will allow the giant planet occurrence rates to be computed at all separations via the combination with direct imaging techniques. The RV search around young stars is a challenge as they are generally faster rotators than older stars of similar spectral types and they exhibit signatures of magnetic activity (spots) or pulsation in their RV time series. Specific analyses are necessary to characterize, and possibly correct for, this activity.
Aims. Our aim is to search for planets around young nearby stars and to estimate the GP occurrence rates for periods up to 1000 days.
Methods. We used the SOPHIE spectrograph on the 1.93 m telescope at the Haute-Provence Observatory to observe 63 $A-M$ young (<400 Myr) stars. We used our Spectroscopic data via Analysis of the Fourier Interspectrum Radial velocities software to compute the RVs and other spectroscopic observables. We then combined this survey with the HARPS YNS survey to compute the companion occurrence rates on a total of 120 young $A-M$ stars.
Results. We report one new trend compatible with a planetary companion on HD 109647. We also report HD 105693 and HD 112097 as binaries, and we confirm the binarity of HD 2454, HD 13531, HD 17250 A, HD 28945, HD 39587, HD 131156, HD 142229, HD 186704 A, and HD 195943. We constrained for the first time the orbital parameters of HD 195943 B. We refute the HD 13507 single brown dwarf (BD) companion solution and propose a double BD companion solution. Two GPs were previously reported from this survey in the HD 113337 system. Based on our sample of 120 young stars, we obtain a GP occurrence rate of $1^{+2.2}_{-0.3}$% for periods lower than 1000 days, and we obtain an upper limit on BD occurrence rate of $0.9^{+2}_{-0.9}$% in the same period range. We report a possible lack of close ($P \in [1; 1000]$ days) GPs around young FK stars compared to their older counterparts, with a confidence level of 90%.

Key words. techniques: radial velocities – stars: activity – binaries: spectroscopic – planetary systems – starspots – stars: variables: general

1. Introduction

More than four thousand exoplanets and brown dwarfs (BDs) have been detected and most of them have been found by transit or radial velocity (RV) techniques[1]. The occurrence rates of these planets are well established for main sequence (MS) and evolved stars, as are some relations between their occurrence rates and their host star characteristics.

The MS late-type stars are the most studied in RV (Cumming et al. 2008; Fernandes et al. 2019; Fischer & Valenti 2005; Santos et al. 2005), together with the evolved stars (Bowler et al. 2009; Johnson et al. 2010; Jones et al. 2016). On the other side of the stellar mass range, early-type MS stars are usually avoided in RV surveys because their optical spectra present fewer spectral lines than late-type stars and because they generally present higher projected rotation velocities ($v \sin i$) than late-type stars. One previous survey was carried out on peculiar AF-type MS dwarfs by Hartmann & Hatzes (2015). A large RV survey of AF-type MS stars was carried out by Borgniet et al. (2019) with the HARPS[2] and SOPHIE[3] instruments. This survey, whose sample

* Tables A.1–A.4 are only available at the CDS via anonymous ftp to cdsarc.u-strasbg.fr (130.79.128.5) or via http://cdsarc.u-strasbg.fr/viz-bin/cat/J/A+A/650/A39

[1] exoplanet.eu

[2] High Accuracy Radial velocity Planet Searcher.

[3] Spectrographe pour l'Observation des Phénomènes des Intérieurs stellaires et des Exoplanètes.

Open Access article, published by EDP Sciences, under the terms of the Creative Commons Attribution License (https://creativecommons.org/licenses/by/4.0), which permits unrestricted use, distribution, and reproduction in any medium, provided the original work is properly cited.

selection criterion was not based on age, contained targets as young as ~100 Myr.

These surveys on MS and evolved stars permit us to identify two correlations between giant planet (GP) occurrence rates and host stellar characteristics. First, there is a positive correlation with the star metallicity for MS FGK stars (Fischer & Valenti 2005; Santos et al. 2005). Then, there is a positive correlation with host star mass. This correlation was observed for evolved stars in RV (Bowler et al. 2009; Johnson et al. 2010; Jones et al. 2016) and for wide orbit planets around young stars in direct imaging (Lannier et al. 2016; Baron et al. 2019). These observations are consistent with the predictions of core accretion models (Kennedy & Kenyon 2008).

Young stars, however, were poorly studied in RV due to their high stellar induced jitter (spots, plages, convection, and pulsations), which can reach amplitudes of up to a few 1 km s^{-1} (Lagrange et al. 2013; Grandjean et al. 2020), larger than the planet's induced signal. Moreover, young stars are generally faster rotators than their older counterparts (Stauffer et al. 2016; Rebull et al. 2016; Gallet & Bouvier 2015). Consequently, several false positive detections were reported around young stars in the past (Huélamo et al. 2008; Figueira et al. 2010; Soto et al. 2015).

One of the remaining questions about planet formation and early evolution is their migration timescales. These timescales can be constrained by the study of young stars. GP formation models predict a formation at a few au (Pollack et al. 1996), yet migration through disk–planet interactions (Kley & Nelson 2012) or gravitational interaction with a third body can allow the planet to finally orbit close to the star (Teyssandier et al. 2019). Massive hot Jupiters (HJs; $m_p \sin i \in [1, 13]$ M_{Jup}, $P \in [1, 10]$ days) are common among exoplanets orbiting solar to late-type MS stars, representing one detected planet out of five (Wright et al. 2012), yet their occurrence rate is low (~1%; Cumming et al. 2008; Wright et al. 2012). While previous RV surveys on young stars (<300 Myr) showed no evidence of the presence of young HJs (Esposito et al. 2006; Paulson & Yelda 2006; Grandjean et al. 2020), three HJs were recently discovered around such young stars with RV (Johns-Krull et al. 2016) and with RV derived from spectropolarimetry (Donati et al. 2016; Yu et al. 2017). Young HJs are also known from transit (Collier Cameron et al. 2010; van Eyken et al. 2012; Mann et al. 2016; David et al. 2019; Rizzuto et al. 2020), and from both transit and RV (Deleuil et al. 2012; Alsubai et al. 2017). In addition, no BDs with periods shorter than 10 days were discovered with RV around young MS stars, although one was discovered from transit (Jackman et al. 2019). The occurrence rates of HJs and short period BDs still need to be constrained at young ages.

We carried out three RV surveys on young stars from A to M types with the final aim of coupling RV data with direct imaging (DI) data, which will allow the computation of detection limits for each target at all separations and then of GP and BD occurrence rates for all separations. The first survey was performed with the High Accuracy Radial velocity Planet Searcher (HARPS; Mayor et al. 2003) on young nearby stars (hereafter HARPS YNS survey) and its results are presented in Grandjean et al. (2020). The second survey was performed with the SOPHIE (Bouchy & Sophie Team 2006) spectrographs on similar young nearby stars. Finally the third survey was performed with HARPS on Sco-Cen stars.

We present in this paper the results of our SOPHIE YNS survey and its combination with the HARPS YNS survey. We describe our SOPHIE survey sample in Sect. 2 and we describe the GP, BD, or stellar companion detections along with their characterizations in Sect. 3. We present the SOPHIE and HARPS combined samples and its statistical analysis, including the occurrence rate computation for GPs and BDs, in Sect. 4. Finally, we present our conclusion in Sect. 5.

2. Description of the SOPHIE survey

2.1. Sample

The initial sample of our SOPHIE YNS survey included 63 stars; most of the targets are part of the SPHERE[4] GTO SHINE[5] survey sample (Chauvin et al. 2017a). The targets were selected according to their declination ($\in$ [+0 : +80] degree), brightness (V < 10), age as found in the literature ($\lesssim$300 Myr for most of them; see Table A.1), and distance (<80 pc) as determined from HIPPARCOS parallax (van Leeuwen 2007). The *Gaia* mission refined the target distances, and one target (HD 48299) is now outside the distance criterion ($d = 95.3 \pm 0.4$ pc; Gaia Collaboration 2018). These criteria ensure the best detection limits for both the SOPHIE RV and SPHERE DI surveys at, respectively, small (typically 2–5 au), and large (further than typically 5 au) separations. The declination criterion was chosen to ensure that the stars' declinations are close to the Haute-Provence Observatory's latitude (+43°55′54″). This ensures a low airmass during most of the observation time, which permits spectra to be obtained with a good signal-to-noise ratio (S/N). This criterion also ensures that most of the targets can be studied with the VLT/SPHERE instrument as the VLT[6] can point up to a declination of +46°. The V-band apparent magnitude criterion was chosen to ensure that the stars are bright enough to obtain spectra with a good S/N. The age and distance criteria were chosen to obtain the best detection limits from direct imaging; young planets are still warm from their formation, and are thus brighter than old ones. This lowers the contrast between them and their host stars. Moreover, nearby stars are better suited for direct imaging. Binary stars with an angular separation on the sky lower than 2 arcsec were not selected to avoid contamination in the spectra from the companion.

Our SOPHIE observations permitted us to measure the projected rotational velocity ($v \sin i$) of the stars in our sample (see Sect. 2.3) and nine of them presented a $v \sin i$ too high (>300 km s^{-1}) to allow RV measurement: HD 56537, HD 87696, HD 97603, HD 116842, HD 126248, HD 159651, HD 177178, HD 203280, and HD 222439. These stars were excluded from our analysis. The ages of the stars in the survey were re-evaluated by the community during the execution of the survey and in some cases the new estimated age was older than our initial age criterion. However, for most of these cases the new estimated age was poorly constrained and the associated uncertainties were huge (up to several Gyr), which does not exclude a low age for these stars. We then chose to keep the stars for which the lower limit on the age is under <500 Myr. As a consequence, five stars were excluded from our analysis due to their old age: HD 2454 (Aguilera-Gómez et al. 2018), HD 48299 (Casagrande et al. 2011), HD 89449 (Gáspár et al. 2016a), HD 148387 (Baines et al. 2018), and HD 166435 (Aguilera-Gómez et al. 2018). Nevertheless, we discuss the RV trend we observe on HD 2454 in Fig. 3. After these different exclusions, 49 targets were available for our analysis.

The spectral type of out targets ranges from A1V to K0V (Fig. 1). Their projected rotational velocities ($v \sin i$) range from

[4] Spectro-Polarimetric High-contrast Exoplanet Research.
[5] The SpHere INfrared survey for Exoplanets.
[6] Very Large Telescope.

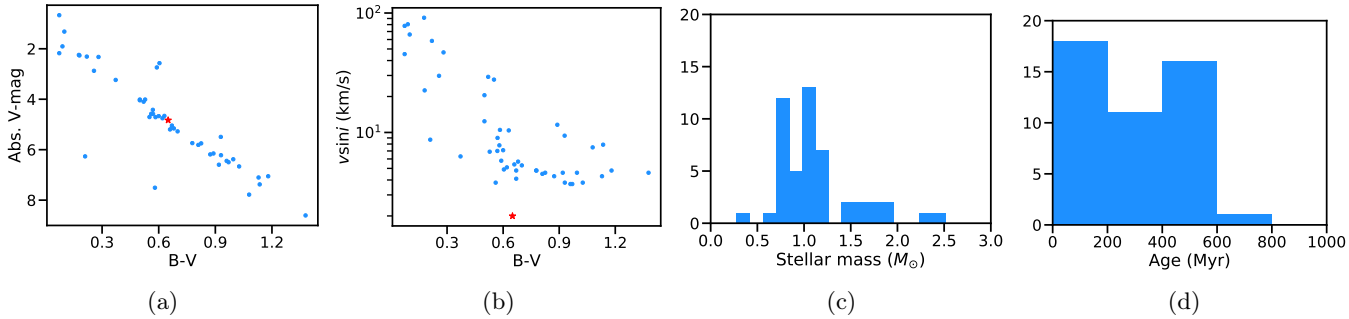

Fig. 1. Main physical properties of our SOPHIE sample. (*a*) Absolute V-magnitude versus $B-V$. Each blue dot corresponds to one target. The Sun is displayed (red star) for comparison. (*b*) $v \sin i$ versus $B-V$ distribution. (*c*) Mass histogram (in $M_\odot$). (*d*) Age histogram.

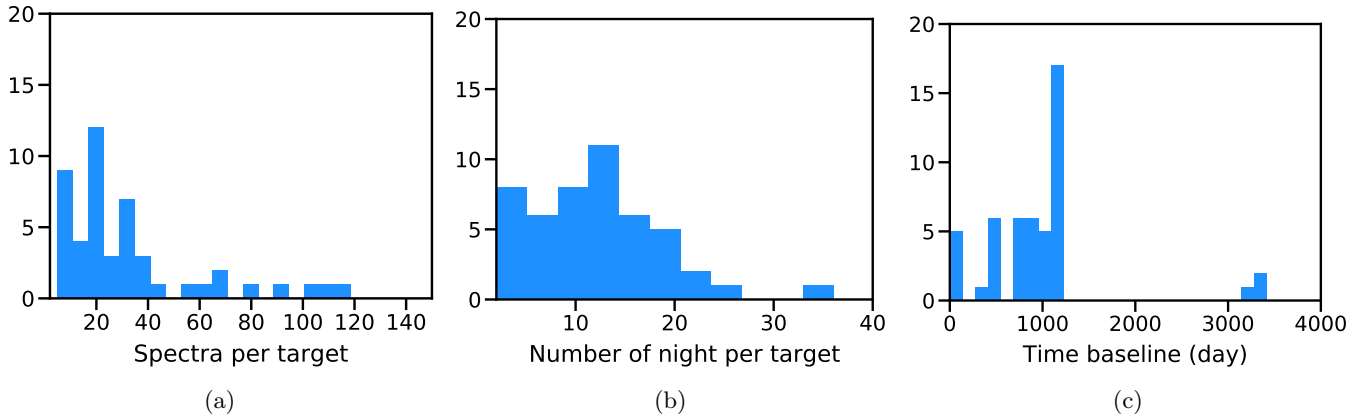

Fig. 2. SOPHIE observation summary. (*a*) Histogram of the number of spectra per target. HD 113337 is not displayed (304 spectra). (*b*) Histogram of the number of nights per target. HD 113337 is not displayed (157 nights). (*c*) Histogram of the time baselines.

1 to 90 km s^{-1}, with a median of 6.9 km s^{-1} (see Sect. 2.3). Their V-band magnitudes range between 2.1 and 10.1, with a median of 7.2. Their masses are between 0.42 and 2.52 $M_\odot$, with a median of 1.07 $M_\odot$ (see Appendix B for mass determination). Our sample includes 13 targets between A0 and F5V ($B-V \in [-0.05 : 0.52[$), 35 between F6 and K5 ($B-V \in [-0.05 : 1.33[$), and 1 between K6 and M5 ($B-V \geq 1.33$). This survey has nine targets in common with the HARPS YNS survey: HD 25457, HD 26923, HD 41593, HD 89449, HD 90905, HD 171488, HD 186704 A, HD 206860, and HD 218396.

We present the main characteristics of our star sample in Fig. 1 and Table A.1.

2.2. Observations

The SOPHIE YNS survey observations were performed between 2013 and 2016. Some stars were previously observed as part of previous surveys made by Borgniet et al. (2014, 2017, 2019). Their time baselines extend to 9 yr.

We adopted the observational strategy presented in Borgniet et al. (2014), which consists in recording two spectra per visit and observing each target on several consecutive nights. This strategy permits us to sample the short-term jitter of late-type stars. For early-type stars the strategy consists in obtaining long sequences of observations (>1.5 h), in order to sample the pulsations of these stars. The number of spectra per target and the number of visits per nights of these stars is then higher than for the late-type stars. The median time baseline of the sample is 975 days (mean time baseline of 975 days), with a median number of spectra per target of 22 (38 on average), spaced on a median number of 12 nights (15 on average; see Fig. 2). Details can be found in Table A.2.

2.3. Observables

We used the Spectroscopic data via Analysis of the Fourier Interspectrum Radial velocities (SAFIR) software to derive the observables from the SOPHIE spectra: RVs and whenever possible the cross-correlation function (CCF), the bisector velocity span (BVS), the star $V \sin i$ (from the full width at half maximum of the CCF), and the log $R'_{\rm HK}$. SAFIR builds a reference spectrum from the median of all spectra available on a given star, and computes the relative RV in the Fourier plane. The computed RVs are then only relative to the reference spectrum, hence we do not compute RVs in heliocentric or barycentric referentials. The efficiency of this method was demonstrated in the search for low-mass companions around AF-type MS stars (Galland et al. 2005b,a).

To filter the bad spectra we used the selection criteria used for the HARPS YNS survey (Grandjean et al. 2020): $S/N_{550\,\rm nm}$[7] $\in [80; 380]$, $sec\ z < 3$, and $\chi^2 < 10$ (Galland et al. 2005b). For faint stars ($V > 8.8$ mag) we included spectra with $S/N_{550\,\rm nm}$ down to 30 as it was the best compromise to include enough spectra to perform our analysis without degrading the RV uncertainties. To determine the main source of RV variability of each star (magnetic activity, pulsations, or companions), we used the correlation between BVS and RV in addition to the shape of the bisectors (Lagrange et al. 2009, 2013; Borgniet et al. 2017).

[7] S/N per pixel between 554.758 and 555.299 nm, estimated with a sampling of 1 pixel every 3 pm.

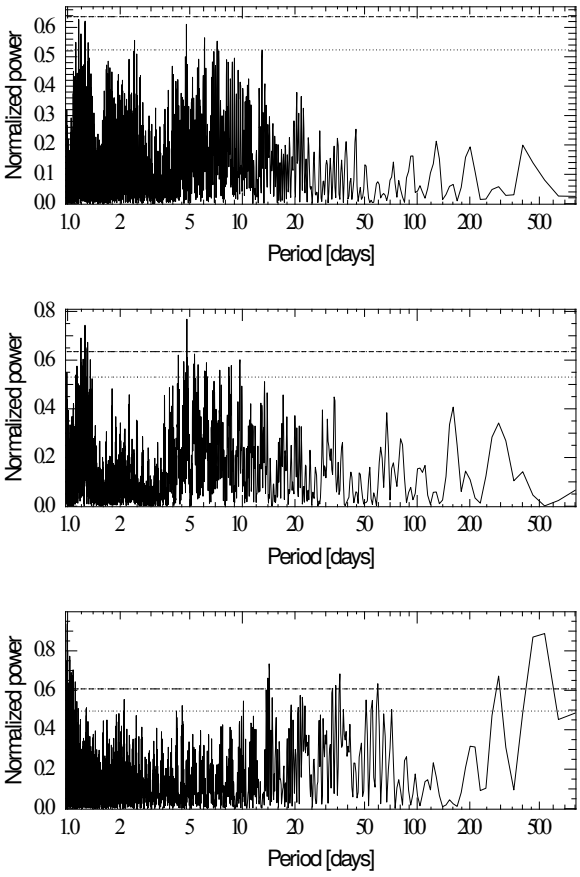

Fig. 3. HD 2454 periodograms. *From top to bottom*: periodogram of the RV residuals of the third-degree polynomial fit, BVS periodogram, time window periodogram. The 10% false alarm probability (FAP) is shown as a dotted line and the 1% FAP as a dashed line.

3. Detected companions in the SOPHIE survey

Among the 49 stars used in our analysis, two planets with periods lower than 1000 days were discovered in the HD 113337 system (Borgniet et al. 2014, 2019). In addition, 13 stars present RVs that are dominated by the signal of a companion. We present their characterizations below.

3.1. RV long-term trends, and stellar binaries

We present here the stars that exhibit a long-term trend, as well as the stars that exhibit a binary signal in their RVs (single-lined spectroscopic binary, SB1) or in their CCF (double-lined spectroscopic binary, SB2). When possible, we characterized the companion that induces the SB1 binary signal with *yorbit* (Ségransan et al. 2011). These characterized SB1 binaries are presented in Fig. 11, and their companions' parameters are summarized in Table 1[8]. In addition, we present the stars with a long-term trend in Fig. 12. For these long-term trends, we estimated the minimum mass needed for a companion to produce the trend. It corresponds to the minimum mass needed for a companion on a circular orbit with a period equal to the time baseline to produce RV variations with an amplitude equal to the drift amplitude. It represents the limit below which a companion on a circular orbit cannot explain the observed total amplitude in the RVs. A companion whose period is equal to the time baseline would produce a signal with visible curvature in our data. The actual period, and thus the actual mass of the companion, is therefore significantly greater than this limit. On the other hand, for a fixed period a companion on an eccentric orbit would produce an identical amplitude with a lower mass, yet with a more visible curvature. A longer period and therefore a higher mass would thus be necessary to produce only a linear trend in the observational window. We can therefore assume that our limit closely corresponds to the limit below which a companion cannot explain the observed total amplitude in the RVs. We present the lower limits of the masses in Table 2. We also verified that the slope induced by the secular drift of these stars is negligible towards the slope of the observed trend. These trends thus cannot be attributed to secular drift.

[8] We provide the uncertainties as given by *yorbit*, but it should be noted that they are often underestimated.

Table 1. Orbital parameters of the characterized binaries.

System	P (yr)	e	$M_p \sin i$ (M_{Jup})
HD 39587	~14	~0.4	~150
HD 195943	3.73 ± 0.03	0.093 ± 0.004	561 ± 4

Table 2. Lower limits on periods and masses for the companions that lead trends.

Star	P(yr)	$M_c(M_{Jup})$
HD 2454	>2.2	>16
HD 17520	>0.01	>7
HD 109647	>3.1	>2
HD 112097	>0.01	>52

Notes. We present these limits for the companions whose periods and masses were not estimated in previous studies.

3.1.1. HD 2454

HD 2454 is an F5V-type star reported as a spectroscopic binary by Escorza et al. (2019). This star is known to present magnetic activity. Rutten (1986) measured a rotation period of 7.8 days from the Ca II variations, while Olspert et al. (2018) measured its harmonic at 3.47 ± 0.01days. We observe a trend with a slope of $222\,\mathrm{m\,s^{-1}\,yr^{-1}}$ over baseline of 805 days with a sign of curvature, in addition to a short term jitter. The minimum mass needed for a companion to induce this trend is $16\,M_{Jup}$. We attribute this trend to the known binary companion. We performed a polynomial fit on the RVs to remove the companion signal (see Fig. 12). We chose a third-degree model as it presented the best reduced χ^2. The residuals have a standard deviation of $11\,\mathrm{m\,s^{-1}}$. The (BVS, RV residuals) diagram is vertically spread. However, the star presents a low sign of activity with a $\langle \log R'_{HK} \rangle$ of −4.89 (with a standard deviation of 0.08). In addition, the periodicities present in the residuals between 4 and 10 days (with a maximum at ~5 days) are also present in the BVS, while they are not present in the time window periodogram. This indicates that the RV jitter could also come from stellar activity. According to the star spectral type (F5V) and its relatively old age (800 ± 300 Myr; Aguilera-Gómez et al. 2018), it is difficult to determine if the RV jitter is dominated by magnetic activity (spots) or pulsations. Due to the weak correlation

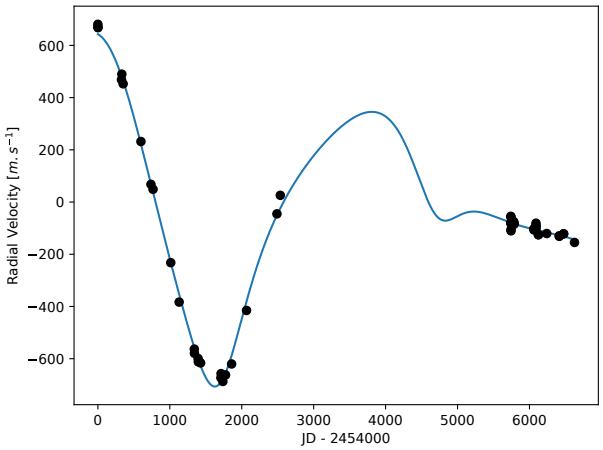

Fig. 4. HD 13507 RVs fit using two Keplerians, performed with Dpass (Lagrange et al. 2019) on the combination of the Perrier et al. (2003) ELODIE RV dataset and our SOPHIE RV dataset.

between the BVS and the RV residuals, we chose to not correct the RV residuals for this correlation.

3.1.2. HD 13507

HD 13507 is a G5V-type star, with a 7.45-day rotation period Wright et al. (2011). Perrier et al. (2003) reported a 52 $M_{\rm Jup}$ companion with a ~3000-day period and an eccentricity of 0.14 from ELODIE RVs. Wilson et al. (2016) refined the orbital solution using the Perrier et al. (2003) RVs together with ELODIE additional RVs. They obtained a period of 4890^{+209}_{-109} days and a $M_{\rm p}\sin i$ of 67^{+8}_{-9} $M_{\rm Jup}$. We observe a trend in our SOPHIE RVs with a slope of 26 m s^{-1} yr^{-1} over a baseline of 886 days. In order to constrain the BD companion parameters, we combined our SOPHIE RV dataset with the ELODIE RV dataset of Perrier et al. (2003) and we fit them together. For this fit we used our Dpass tool, which is based on an evolutionary algorithm (Lagrange et al. 2019), and we took into account an offset between the two datasets. Our fit does not confirm the Perrier et al. (2003) and Wilson et al. (2016) solutions, and it clearly shows that the system is not single. We then considered a two-planet system[9], and found a possible solution including two BD companions of lower masses, 0.02 and 0.03 $M_\odot$ (21 $M_{\rm Jup}$ and 31 $M_{\rm Jup}$, respectively) orbiting at 4.2 (⇔ 8.3 yr) and 5.4 *au* (⇔ 12.1 yr), and with low eccentricities, 0.27 and 0.2, respectively (cf. Fig. 4). Other degenerate solutions may exist, which prevents us from giving a proper estimate of the uncertainties on these parameters. We note that such companions could be detected in high-contrast imaging, and that the orbits are close to 3:2 resonance. We also note that this solution should be taken with caution, given the limited number of data points available.

3.1.3. HD 13531

HD 13531 is a G7V-type star, with a 7.49-day rotation period (Wright et al. 2011), that presents an IR excess (McDonald et al. 2012). The radius of the corresponding warm disk was estimated at 1.78 au (Gáspár et al. 2016a). We observe a trend in the RVs with a slope of 37 m s^{-1} yr^{-1} over a baseline of 882 days. The minimum mass needed for a companion to induce this trend is 3 $M_{\rm Jup}$. Metchev (2006) discovered a low-mass star candidate companion by direct imaging with a semimajor axis of 18.6 au (81 yr) and a mass estimated at 0.19 $M_\odot$. For circular and edge-on orbits the total amplitude in RV of this companion is 2.65 km s^{-1}, and the mean annual variation is 65 m s^{-1} yr^{-1}, which is on the order of magnitude of the slope of the trend we observe. We thus attribute this RV trend to this companion. The residuals of a linear regression show a jitter with an amplitude of 11 m s^{-1} (see Fig. 12). These residuals show a significant correlation between the BVS and the RVs (Pearson = −0.54, $p_{\rm value}$ = 0.1%), which indicate that the jitter is due to stellar activity (spots).

[9] No constraint was put on the two companion properties, except on the eccentricities that were constrained to be lower than 0.3. Both eccentricities were regularized under the arbitrary assumption that eccentricities follow a normal law (0, 0.1).

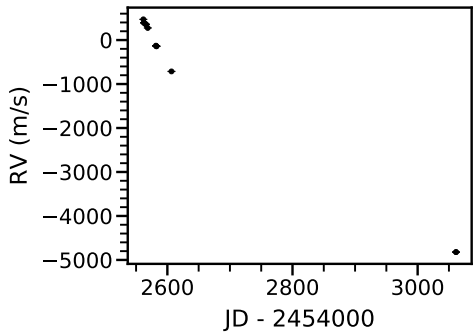

Fig. 5. HD 28495 RV time variations.

3.1.4. HD 17250

HD 17250 is known as a hierarchical multiple system composed of four stars (Tokovinin 2014). The main star, HD 17250 A, presents an IR excess (McDonald et al. 2012) and a spectroscopic binary companion (Tokovinin 2014). We observe a trend of 1145 m s^{-1} over 5 days. According to the amplitude of the signal on a such short timescale, it is unlikely that the signal is produced by a companion, other than the one reported by Tokovinin (2014), as it would require the latter to produce a signal of even greater amplitude over a longer timescale. We thus attribute this signal to the spectroscopic companion reported by Tokovinin (2014). Our data are too sparse to study the residuals of a linear regression on the RVs (see Fig. 12).

3.1.5. HD 28495

HD 28945 is a G0V-type star that was reported as a spectroscopic binary by Nordström et al. (2004), then as an astrometric binary from HIPPARCOS proper motion (Makarov & Kaplan 2005; Frankowski et al. 2007). We observe a variation in the RVs with an amplitude of 5.3 km s^{-1} over 500 days with a sign of curvature. However, this sign of curvature relies on only two data points (see Fig. 5). We attribute these RV variations to the known stellar companion, but more data points are needed to characterize the system.

3.1.6. HD 39587

HD 39587 (χ^1 Orionis) has been known as a binary since 1978 from absolute astrometry; it is composed of a solar-like G0V star and a low-mass star companion on a close and nearly edge-on orbit ($i = 95°$) (Lippincott & Worth 1978). The orbital parameters of the stellar companion were refined by combining radial velocity and absolute astrometry by Han & Gatewood (2002). They obtained a period of 5156.7 ± 2.5 days, an eccentricity

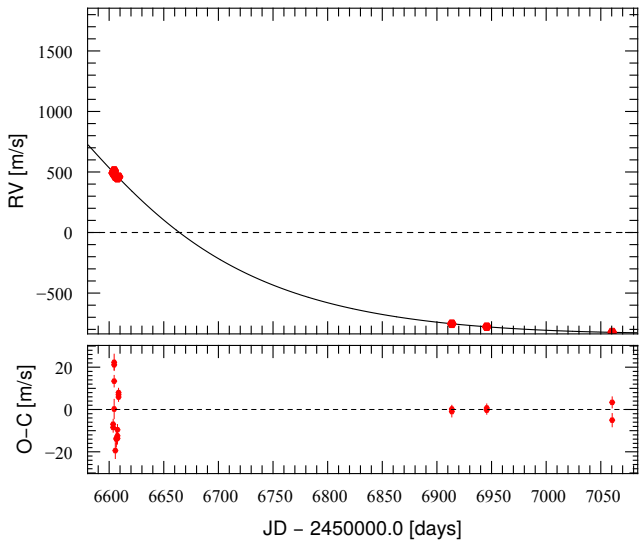

Fig. 6. HD 39587 RVs best fit with one Keplerian and its residuals.

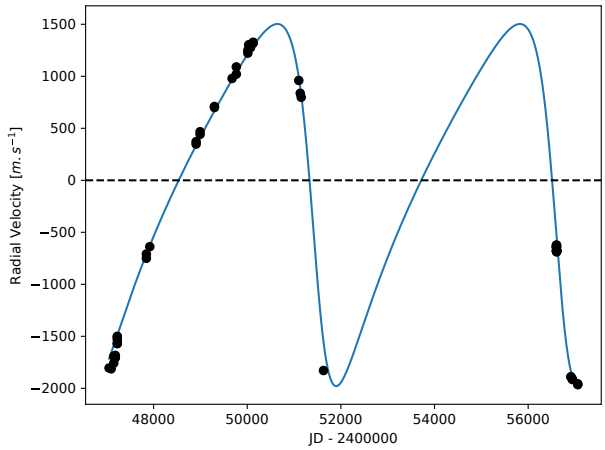

Fig. 7. HD 39587 RVs fit using one Keplerian, performed with Dpass (Lagrange et al. 2019) on the combination of the Han & Gatewood (2002) Lick Observatory RV dataset and our SOPHIE RV dataset.

of 0.451 ± 0.003, and a mass of $0.15 \pm 0.02\,M_{\odot}$ for the companion. This companion was then directly imaged in 2002 by Koenig et al. (2002). We observe the signal of the stellar companion in our RVs. We use *yorbit* to fit the RVs with one Keplerian model. For this fit we adopt a mass of $1.07\,M_{\odot}$ for the primary (Tokovinin 2014). We obtain a period of 5600 ± 3400 days (6.5 au, 750 mas), an eccentricity of 0.89 ± 0.15. However, the $M_{\rm p} \sin i$ is not constrained in this fit. We present this fit in Fig. 6 and the (BVS, RV) diagram of its residuals in Fig. 11). Our solution is consistent at 1σ with previous literature values in terms of period, but not in terms of eccentricity. Our solution is more eccentric, which leads to a lower mass for the companion. We see a strong correlation between the BVS and the RVs of the spectra taken after 2014, which indicates that they might be altered by the activity of the star (spots). This can explain the strong difference in eccentricity between our values and those found in the literature.

We then combined our SOPHIE RV dataset with the Lick Observatory RV dataset of Han & Gatewood (2002) in order to perform a joined fit with our Dpass tool (Lagrange et al. 2019) using a singular Keplerian model. We also adopted a mass of $1.07\,M_{\odot}$ (Tokovinin 2014) for the primary and we took into account an offset between the two datasets. We added quadratically $10\,{\rm m\,s^{-1}}$ to the error bars of our SOPHIE RV dataset to take into account that the stellar origin jitter is badly sampled after 2014. We present this fit in Fig. 7. We obtain a mass of $0.15\,M_{\odot}$, an eccentricity of 0.44, and a period of 5180 days for the companion, which is similar to the estimation of Han & Gatewood (2002) on these parameters. However, as other degenerate solutions may exist in our fit we cannot make a proper estimation of the uncertainties on the value of the parameters we estimate, which prevent us from making a better comparison between our results and the results of Han & Gatewood (2002).

3.1.7. HD 105963

HD 105963 is a known wide-orbit binary (Lépine & Bongiorno 2007) with a 13.5″ separation (Durkan et al. 2016). We observe a double component in the CCF. The field of view of the SOPHIE fiber is 3″ (Perruchot et al. 2011), so this component cannot come from the wide separation companion. We thus report HD 105693 A as a SB2.

3.1.8. HD 109647

HD 109647 is a K0V-type star that presents an infrared excess (McDonald et al. 2012). We observe a trend in the RVs with a slope of $17\,{\rm m\,s^{-1}\,yr^{-1}}$ over a baseline of 1147 days. The minimum mass needed for a companion to induce this trend is $2\,M_{\rm Jup}$. The residuals of a linear regression show a jitter with an amplitude of $22\,{\rm m\,s^{-1}}$ (see Fig. 12). These residuals show a significant correlation between the BVS and the RVs ($Pearson = -0.6$, $p_{\rm value} = 0.2\%$), which indicates that the jitter is due to stellar activity (spots). The age of the system is 412 Myr (Stone et al. 2018), which does not allow us to confirm this companion by direct imaging with the current instrumentation.

3.1.9. HD 112097

HD 112097 is an A7III-type star. We observe a trend of $8\,{\rm km\,s^{-1}}$ over 3 days. The minimum mass needed for a companion to induce this trend is $52\,M_{\rm Jup}$. We report thus HD 112097 as a spectroscopic binary. Our data are too sparse to study the residuals of a linear regression (see Fig. 12).

3.1.10. HD 131156

HD 131156 (ξ *Boo*) is a G7V-type star known to be a visual binary since 1950 (Muller 1950). Stone et al. (2018) measured a separation of 4.94″ (33 au) and estimated the mass of the two components as $m1 = 1\,M_{\odot}$ and $m2 = 0.7\,M_{\odot}$. We observe a trend with a slope of $35\,{\rm m\,s^{-1}\,yr^{-1}}$ over a baseline of 1154 days. The maximum annual RV variation that HD 131156 B can apply to its host star is $76\,{\rm m\,s^{-1}\,yr^{-1}}$, which is greater than the slope of the trend we observe. We thus attribute the RV trend we observe to HD 131156 B. The residuals of a linear regression show a jitter with an amplitude of $30\,{\rm m\,s^{-1}}$ (see Fig. 12). These residuals show a significant correlation between the BVS and the RVs ($Pearson = -0.88$, $p_{\rm value} < 4 \times 10^{-12}\%$), which indicates that the jitter is due to stellar activity (spots).

3.1.11. HD 142229

HD 142229 is a G5V-type star known to present an IR excess (McDonald et al. 2012) and a RV trend (Nidever et al. 2002). Gáspár et al. (2016a) estimated the warm disk radius at 1.94 au from 24 µm *Spitzer* data. From additional RV data Patel et al. (2007) estimated a period greater than 16.4 yr and an $M_{\rm p} \sin i$

greater than 150 $M_{\rm Jup}$ for the companion. We observe a trend with a slope of 71 m s^{-1} yr^{-1} over a baseline of 1111 days. This trend is compatible with the solution obtained by Patel et al. (2007), we thus attribute this trend to HD 142229 B. The residuals of a linear regression present a standard deviation of 21 m s^{-1} with a weak correlation between BVS and RV (see Fig. 12). According to the star spectral type we attribute this jitter to spots.

3.1.12. HD 186704 A

HD 186704 is a known binary system with a companion at 10 arcsec (Zuckerman et al. 2013). Nidever et al. (2002) reported a trend in the RVs of 88 ± 8 m s^{-1} d^{-1} with a negative curvature based on four observations spaced over 70 days for HD 186704 AB. Tremko et al. (2010) observed a change in the RVs of 4200 m s^{-1} in 8682 days on HD 186704 A. Finally, Tokovinin (2014) reported HD 186704 A as hosting a spectroscopic binary (SB) companion with a 3990 – *day* period. We reported in Grandjean et al. (2020) a trend in the HARPS RVs with a slope of 275 m s^{-1} yr^{-1} over a baseline of 450 days baseline (data taken between 2014 and 2015). This trend was attributed to the known SB companion. We observe in the SOPHIE RVs a trend with a slope of 268 m s^{-1} yr^{-1} over a baseline of 1042 days (data taken between 2013 and 2016). It emphasizes the consistency between SOPHIE and HARPS data. The residuals of a linear regression show a jitter with an amplitude of 38 m s^{-1} (see Fig. 12). These residuals show a significant correlation between the BVS and the RVs (*Pearson* = −0.64, $p_{\rm value} = 0.2\%$), which indicates, in addition to the star's relatively fast rotation ($P_{\rm rot} = 3.511$ days; Kiraga 2012) and Ca II H and K activity ($\langle \log R'_{\rm HK} \rangle = -4.32$), that the measured jitter is likely due to stellar activity (spots).

3.1.13. HD 195943

HD 195943 (η *Del*) is an A3IV-type star that was reported as a binary on the basis of HIPPARCOS proper motion (Makarov & Kaplan 2005; Frankowski et al. 2007). We get a good coverage of this companion signal in RV. Our best *yorbit* fit gives a period of 1363 ± 11 days (3.73 yr), an eccentricity of 0.093 ± 0.004, and a $M_{\rm p} \sin i$ of 561 ± 4 $M_{\rm Jup}$ (0.54 $M_{\odot}$). We present our fit in Fig. 8. For this fit we assumed that the 2.25 $M_{\odot}$ mass estimated from an evolutionary model by Zorec & Royer (2012) corresponds to the primary mass. However, this mass estimation might be affected by the binary companion. This will thus lead to an overestimation of the $M_{\rm p} \sin i$ and an underestimation of the period in our fit. The residuals of the fit show a vertical spread of the (BVS, RV) diagram, and can thus be attributed to pulsations (see Fig. 11).

3.1.14. HD 218738

HD 218738 (KZ Andromedae) is known to be the component of a common proper motion binary along with HD 218739. HD 218738 is also known as a double line binary with a period of 3.03 days (Bopp & Fekel 1975; Fekel et al. 2017). We observe this double component in our spectra. However, our data are too sparse to characterize this binary.

3.2. Giant planets: HD 113337

HD 113337 is an F6V-type star that presents an IR excess (Rhee et al. 2007). The corresponding debris disk was resolved by Su et al. (2013). A first planetary companion was discovered

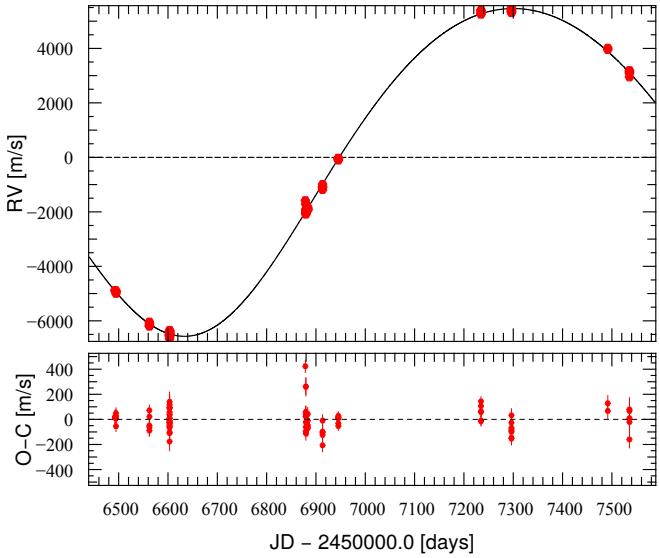

Fig. 8. HD 195943 RVs best fit with one Keplerian and its residuals.

from previous SOPHIE surveys, in addition to a long-term variation attributed to stellar activity (Borgniet et al. 2014). The additional data obtained during the SOPHIE YNS survey permitted Borgniet et al. (2019) to discover that the long-term variations are due to a second companion. The parameters of the two companions are $P_1 = 323 \pm 1$ days, $M_{p1} \sin i_1 = 3 \pm 0.3$ $M_{\rm Jup}$ and $P_2 = 3265 \pm 134$ days, $M_{p2} \sin i_2 = 6.9 \pm 0.6$ $M_{\rm Jup}$.

3.3. Detected companion summary

Over the 49 stars of our analysis a system composed of two planets with $P < 1000$ days was discovered (Borgniet et al. 2014, 2019). In addition, we observed ten single-lined spectroscopic binary systems and two double-lined binary systems, eight of which were already reported in the literature, while two were unknown (HD 105693 B, HD 112097 B). Finally, we report a long-term trend compatible with a planetary companion on HD 109647.

3.4. Known giant planet non-detections

Some of our targets are known to host confirmed or debated giant planets. We present here the non-detection of these companions.

3.4.1. HD 128311

HD 128311 is a K0V-type star that is known to host two planets in 2:1 mean motion resonance. The first was detected by Butler et al. (2003), who estimated its period at 422 days and its $M_{\rm p} \sin i$ at 2.57 $M_{\rm Jup}$. Vogt et al. (2005) confirmed this companion and discovered a second one. They estimated their periods to be 458.6 days and 928 days, and $M_{\rm p} \sin i$ at 2.18 $M_{\rm Jup}$ and 3.21 $M_{\rm Jup}$, respectively. They also found a periodicity in the photometry of the star with a period of 11.53 days. Wittenmyer et al. (2009) confirmed the two planets with the high-resolution spectrograph of the *Hobby–Ebberly* telescope, and they estimated their period at 454.2 ± 1.6 days and 923.8 ± 5.3 days, and their $M_{\rm p} \sin i$ at 1.45 ± 0.13 $M_{\rm Jup}$ and 3.24 ± 0.1 $M_{\rm Jup}$, respectively. They noted a strong periodicity in the residuals of their two-Keplerian fit, with a period of 11.5 days, which corresponds to the rotation period of the star previously measured by Vogt et al. (2005). Finally, McArthur et al. (2014) combined *Hubble* Space

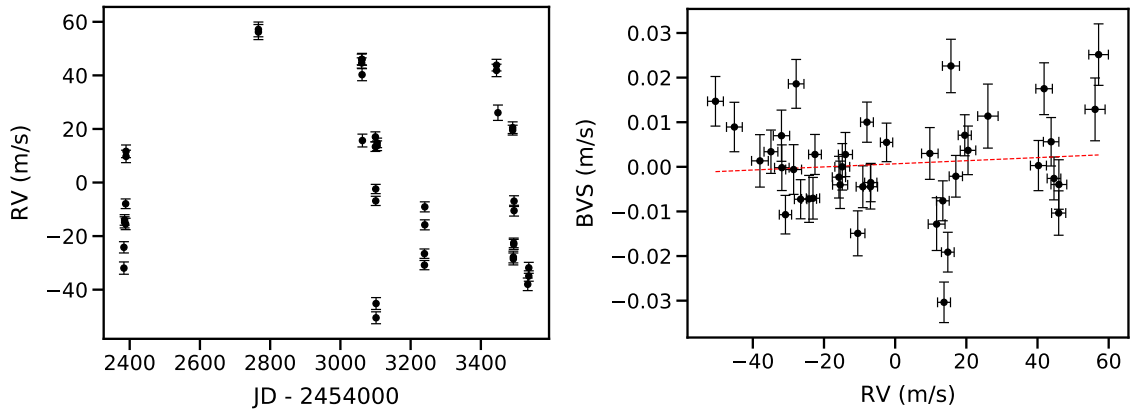

Fig. 9. HD 128311 RV variations (*left*) and (BVS, RV) diagram (*right*).

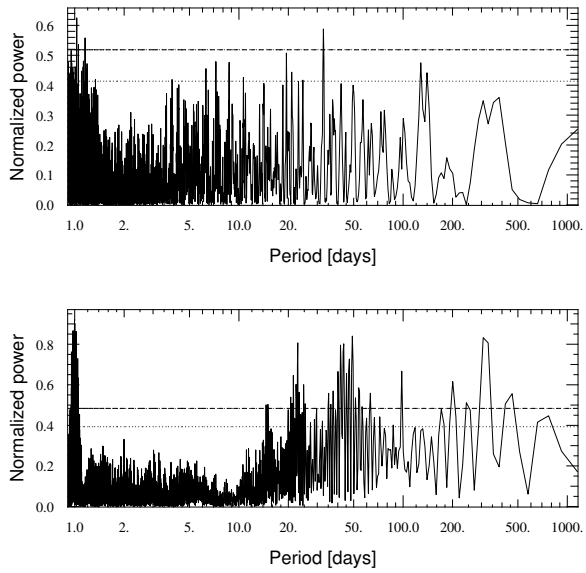

Fig. 10. HD 128311 periodograms *Top*: RVs periodogram. *Bottom*: time window periodogram. The 10% false alarm probability (FAP) is shown as a dotted line and the 1% FAP as a dashed line.

Telescope astrometry and additional RVs from the *Hobby–Ebberly* telescope spectrograph to constrain the inclination of the system. They find an inclination of 55.95 ± 14.55° and a true mass of $3.789^{+0.924}_{-0.432}$ $M_{\rm Jup}$ for HD 128311 c.

Our data show parallel bisectors and a flat (BVS, RV) diagram ($Pearson = 0.09$, $p_{\rm value} = 56\%$, see Fig. 9), which indicates the presence of companion. However, we do not recover the two known companions in our data. The periodogram of our SOPHIE RVs show a strong signal at 30 days, a weak signal near 450 days, and a very weak signal near 900 days (see Fig. 10). This 30-day period could be a multiple of the rotation period seen in the photometry. We attribute thus this period to magnetic activity. The periodogram of the time window of our observations shows a strong signal near 450 days, which explains why we do not recover HD 128311 b (see Fig. 10). Moreover, our time baseline is only 1153 days and our data are sparse (41 spectra), which explains why we do not recover HD 128311 c.

3.4.2. BD+20 1790

BD+20 1790 is a K5V star for which the presence of a giant planet was refuted. Hernán-Obispo et al. (2010) first reported a companion with a period of 7.78 days from RV, along with a 2.28 – day period in the photometry of the star. The companion was then refuted by Figueira et al. (2010) as the star presented a strong BVS versus RV correlation, which indicated that the RV signal were dominated by the stellar activity (spots). Hernán-Obispo et al. (2015) reanalyzed the RV data and found that the RV variations were composed of three signals: the first with a period of 2.8 days that was linked to the photometric rotation period; the second with a period of 4.36 days that was linked to the synodic period of the star–planet system; and the third with a period of 7.78 days, which they attributed to the companion. Gagné et al. (2016) combined the Hernán-Obispo et al. (2010) and Figueira et al. (2010) data with their CSHELL data, and did not identify any significant periodicity in them or in any combination of them. Finally, Carleo et al. (2018) used multiband spectroscopy to show that the RV variations of BD+20 1790 are chromatic, ruling out the companion.

In our SOPHIE RVs we observe a ~1 km s^{-1} amplitude variation, which is consistent with the previous literature. The BVS are strongly correlated to the RVs, which is consistent with the Figueira et al. (2010) analysis. However, we have too few spectra (10) to permit the characterization of this stellar signal.

4. SOPHIE and HARPS YNS combined survey analysis

In order to improve the statistics of GPs around young stars, we combine the SOPHIE YNS survey with the HARPS YNS survey (presented in Grandjean et al. 2020). This combination is presented below.

4.1. Sample

The HARPS survey consist of 89 targets, 9 of which are in common with the SOPHIE survey (see Sect. 2.1), leading to a total of 143 distinct targets in the combined survey.

In this combined survey, 19 spectroscopic binary systems were highlighted (17 SB1, 2 SB2). Two planets with $P <$ 1000 days were discovered in the HD 113337 system (Borgniet et al. 2014, 2019). One long-period ($P >$ 1000 days) sub-stellar candidate was discovered in the HD 206893 system (Grandjean et al. 2019). Finally, one star presents a trend compatible with a GP companion signal.

For the targets observed in both surveys we chose to use the instrument for which we have the larger number of spectra and the longer time baseline (SOPHIE: HD 89449, HD 171488,

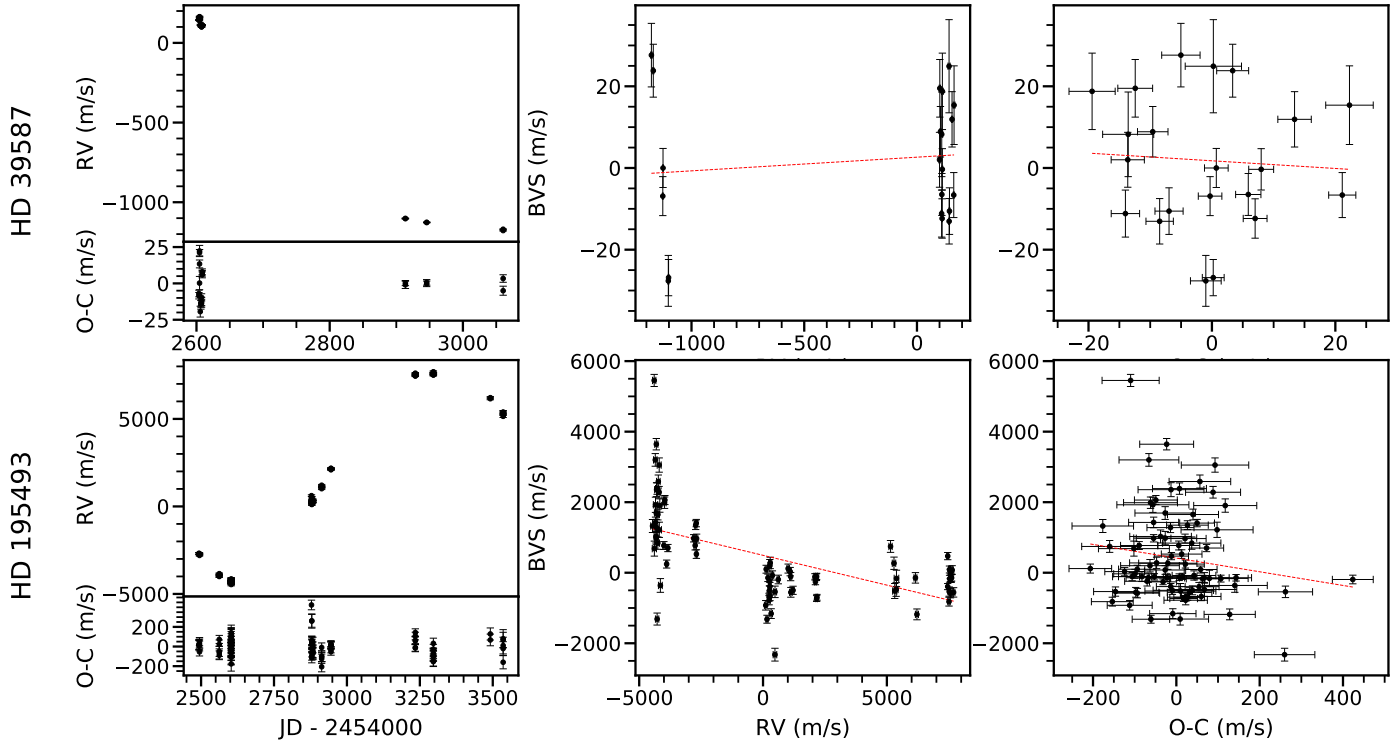

Fig. 11. Binary star RV analysis. *First column*: RV time variations (*top*) and its Keplerian fit residuals. These fits are presented in Fig. 6 for HD 39587 and in Fig. 8 for HD 195943. *Second column*: BVS versus RVs (black) and its best linear model (red dashed line). *Third column*: BVS versus RV residuals and its best linear model (red dashed line).

HD 186704 A, HD 206860. HARPS: HD 25457, HD 26923, HD 41593, HD 90905). For HD 218396 the SOPHIE and HARPS time baselines are similar. In this case we favored the number of spectra over the time baseline as it presents a better sampling of the jitter. We thus used the SOPHIE data for HD 218396 as it presents twice the number of spectra even though the time baseline is 30% shorter than for HARPS data.

We do not combine our HARPS and SOPHIE RV data for these targets, as it is not possible to determine an accurate value of the offset between the two datasets (as each dataset is relative to its respective median spectra). Moreover, our detection limits are based on RVs periodograms (see Sect. 4.4) and the uncertainty on the offset would lead to a biased combined periodogram, and thus to biased detection limits.

From the HARPS YNS sample we excluded the targets that were excluded in Sect. 4.3 of Grandjean et al. (2020). From the SOPHIE YNS survey we excluded the star excluded in Sect. 2.1. In addition, we excluded the binary stars for which the companion signal could not be fitted: HD 28495, HD 105963, and HD 218738. This leads to a total of 120 targets in the combined survey. All the following figures will present the HARPS targets in black and the SOPHIE targets in blue.

The targets of our final sample have spectral types that range from A0V to M5V (Fig. 13). This sample includes 32 targets between A0 and F5V ($B-V \in [-0.05 : 0.52[$, hereafter AF sub-sample), 79 between F6 and K5 ($B-V \in [-0.05 : 1.33[$, hereafter FK sub-sample), and 9 between K6 and M5 ($B-V \geq 1.33$, hereafter M sub-sample). Their projected rotational velocity ($v \sin i$) ranges from 1.7 to 120 km s^{-1}, with a median of 7.1 km s^{-1}. Their V-band relative magnitude ranges between 1.2 and 10.1, with a median of 7.6. Their masses are between 0.42 and 2.74 $M_\odot$, with a median of 1.0 $M_\odot$ (see Appendix B for masses determination). The AF sub-sample presents a median mass of 1.62 $M_\odot$ with a standard deviation of 0.38 $M_\odot$, the FK sub-sample presents a median mass of 0.93 $M_\odot$ with a standard deviation of 0.19 $M_\odot$, and the M sub-sample presents a median mass of 0.6 $M_\odot$ with a standard deviation of 0.08 $M_\odot$.

The distances of the stars in our sample range between 3 and 113 pc, with a median of 28 pc (see Fig. 14, Gaia Collaboration 2018).

The median age of the sample is 149 Myr (see Appendix B for age determination). The uncertainties on the ages range from several million years to several hundred million years. We chose two ways to represent them. First, we present a histogram of the ages in Fig. 15a. We chose the histogram bin to be larger than the median uncertainty on the age of the star in the survey. This ensures that the real ages of most of the stars in the survey are within the range where they were counted. Second, we considered an alternative way to present the age of the survey that we call the histogram of the possible age. It is a histogram where we count in each bin the number of stars for which the bin is within their errorbars. It represents the ranges of possible values for the ages of the stars. As the stars are counted several times, this histogram give only qualitative information. We present the histogram of the possible age of the combined sample in Fig. 15b. We can observe several peaks corresponding to different moving groups: ~40 Myr (Tucana/Horlogium, Carina, Columba, Argus; Bell et al. 2015), ~130−150 Myr (AB Doradus; Bell et al. 2015), and 250 Myr (Hercules/Lyraes; Eisenbeiss et al. 2013).

Metallicity measurements are only available for 86 of our targets. Their metallicities are close to the solar value, with a median of 0.03 dex (mean of 0.03 dex) and a standard deviation of 0.14 dex. We observe no statistically significant correlation between the metallicity and the $B-V$ nor between the metallicity and the stellar mass in our sample. We present the metallicity of the combined sample in Fig. 16.

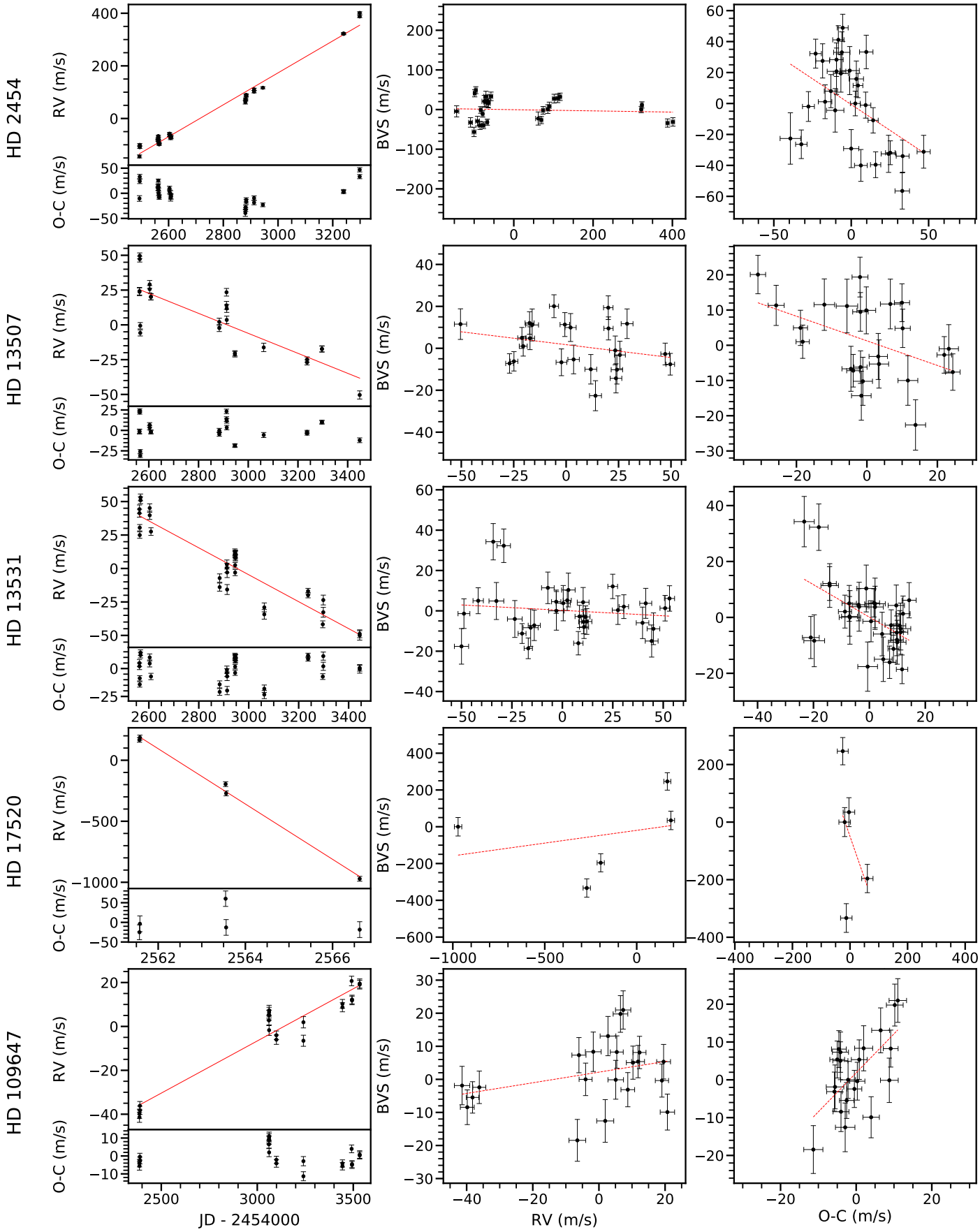

Fig. 12. Stars with trend RV analysis. *First column*, *top*: RV time variations (black) with the model of its linear regression (red line); *bottom*: residuals of the linear regression. *Second column*: BVS versus RVs (black) and its best linear model (red dashed line). *Third column*: BVS versus RV residuals and its best linear model (red dashed line).

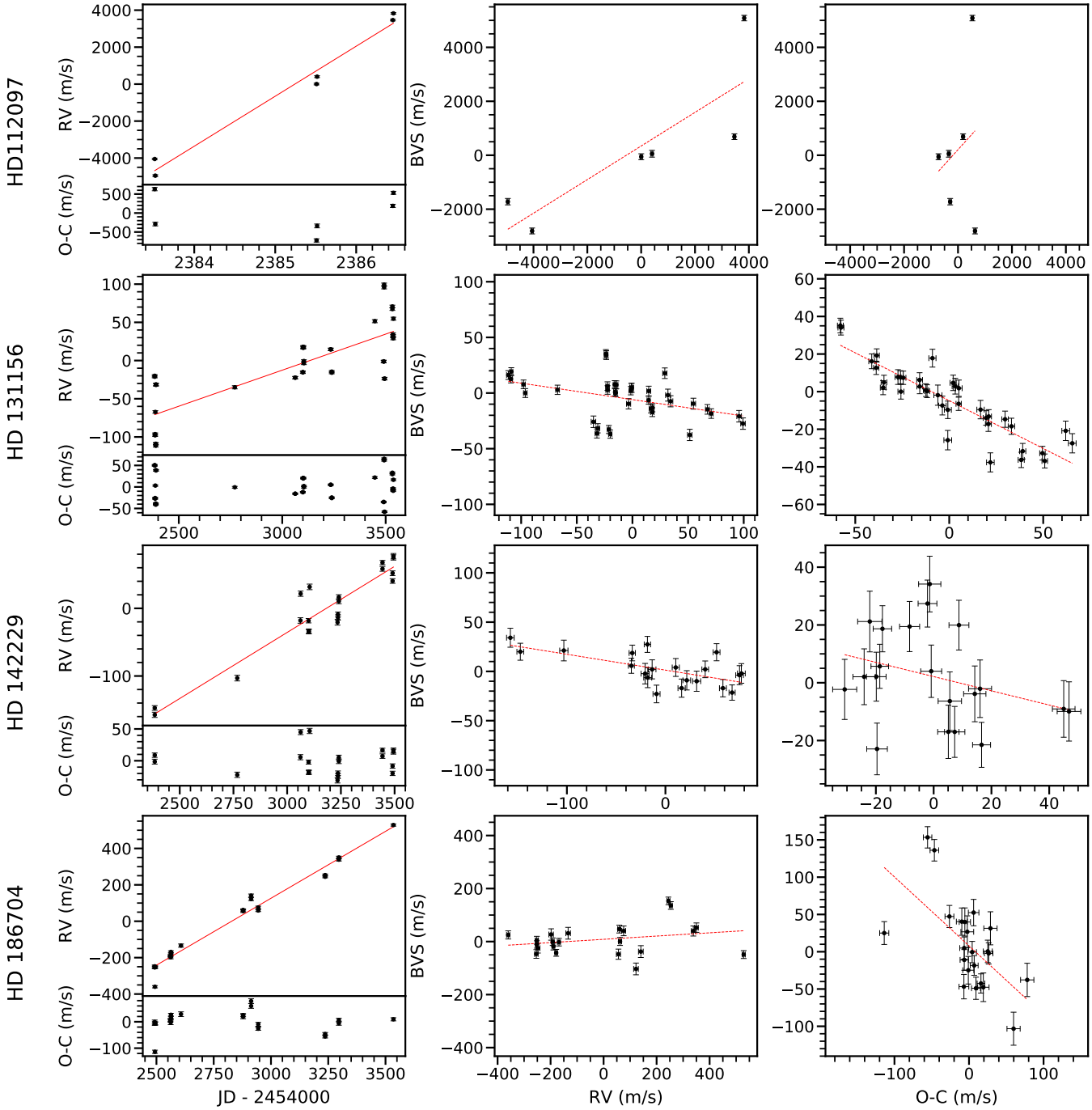

Fig. 12. continued.

The median time baseline is 2621 days (mean time baseline of 2493 days), with a median number of spectra per target of 25 (92 on average) spaced over a median number of 13 nights (18 on average, Fig. 17).

Details can be found in Tables A.1, A.3, A.2, and A.4 (Tables A.3 and A.4 being updated versions of Tables A.1 and A.2 presented in Grandjean et al. 2020).

4.2. Stellar intrinsic variability

The jitter observed in the RV time series of our combined sample is mainly caused by pulsations for early-type stars (from A to F5V), and by spots and faculae for late-type stars ($>F5V$). Those two regimes can be distinguished from each other as stars with pulsations show a vertically spread (BVS, RV) diagram, whereas stars with spots present a correlation between BVS and RV (Lagrange et al. 2009). The main origin of RV jitter is reported in Tables A.2 and A.4 for each target of the HARPS YNS and SOPHIE YNS surveys, respectively. The distinction between stars with pulsations (labeled "P" in these tables) and stars with spots (labeled "A") was based on the stellar spectral type, the shape of the bisectors (Lagrange et al. 2009), and the (BVS, RV) diagram shape as exposed above.

The stars of the combined survey present a strong jitter. After the removal of the companion's signal (see Sect. 3) and the HD 217987 secular drift (see Grandjean et al. 2020), the ratio of the RV rms to the mean RV uncertainty is between 120 and 1, with a median at 12. The median of the RV rms is 44 m s^{-1} (129 m s^{-1}

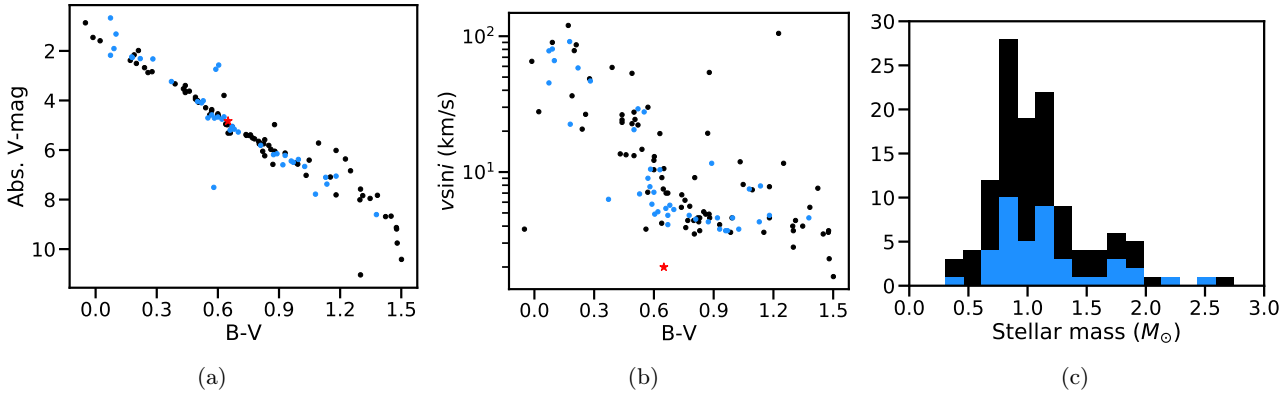

Fig. 13. Main physical properties of our combined HARPS and SOPHIE YNS sample. HARPS targets related data are in black and SOPHIE related data are in blue. The HARPS (black) histogram and the SOPHIE (blue) histogram are stacked. (*a*) Absolute V-magnitude versus $B-V$. Each dot corresponds to one target. The Sun is displayed (red star) for comparison. (*b*) $v \sin i$ versus $B-V$ distribution. (*c*) Histogram of the star masses (in $M_\odot$).

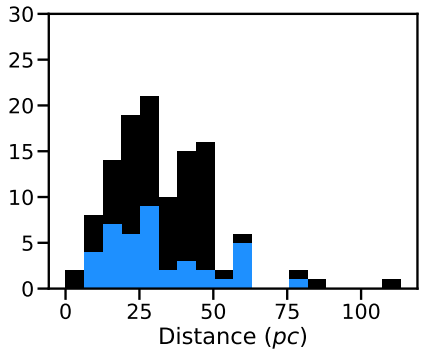

Fig. 14. *Gaia* DR2 (Gaia Collaboration 2018) distance histogram of our combined HARPS and SOPHIE YNS sample. The HARPS (black) histogram and the SOPHIE (blue) histogram are stacked.

on average). We display in Fig. 18 the mean RV uncertainty versus $B-V$, versus $v \sin i$, and versus M_*, of the combined sample. We also display the RV rms versus $B-V$ and versus age in Fig. 19. The mean RV uncertainty is strongly correlated with $v \sin i$ ($Pearson = 0.78$, $p_{\rm value} < 6 \times 10^{-26}\%$). The correlation of the combined survey is stronger than for the HARPS YNS survey alone ($Pearson = 0.69$).

Out of 120 stars in our sample, 110 present variations in their Ca lines, which confirms the presence of stellar activity for a large number of targets. The median $\langle \log R'_{\rm HK} \rangle$ of our sample is −4.3 with a standard deviation of 0.2. Of these targets, 4 present signs of low activity ($\langle \log R'_{\rm HK} \rangle < -4.75$), 85 are active ($-4.75 < \langle \log R'_{\rm HK} \rangle < -4.2$), and 21 present signs of high activity ($\langle \log R'_{\rm HK} \rangle > -4.2$). The median of the standard deviations of the $\langle \log R'_{\rm HK} \rangle$ of the stars of the sample is 0.03 (mean of 0.04). We present in Fig. 20 $\langle \log R'_{\rm HK} \rangle$ versus $B-V$.

4.3. RV correction for further analysis

We used the method presented in Grandjean et al. (2020) to correct the RVs of the SOPHIE stars from their jitter and from their companion signal: for the stars for which the RVs are dominated by spots (labeled A in Table A.2), we corrected the RVs from the (BVS, RV) correlation using the Melo et al. (2007) method. For the stars that present a trend (see Sect. 3.1), we applied a linear regression on their RVs. If the residuals presented a correlation between the BVS and the RVs, we corrected them for this correlation (Melo et al. 2007). For the binary star for which it was possible to fit the companion signal (see Sect. 3.1), we worked on the residuals. If the residuals presented a correlation between the BVS and the RVs we corrected them for this correlation (Melo et al. 2007).

For the HARPS stars we used the corrected data presented in Grandjean et al. (2020).

4.4. Detection limits

We used the local power analysis (LPA; Meunier et al. 2012; Borgniet et al. 2017) to compute the $m_{\rm p} \sin i$ detection limits for periods between 1 and 1000 days in the GP domain (between 1 and 13 $M_{\rm Jup}$), and in the BD domain (between 13 and 80 $M_{\rm Jup}$). The LPA method determines, for all periods P, the minimum $m_{\rm p} \sin i$ for which a companion on a circular orbit[10] with a period P leads to a signal consistent with the data; this is done by comparing the synthetic companion maximum power of its periodogram to the maximum power of the data periodogram within a small period range around the period P. For a given star the detection limit is infinite for periods greater than its time baseline. We made this choice because the high jitter and the moderate number of spectra per target do not provide a strong constraint on a companion signal that has a period greater than the time baseline.

We then computed the completeness function $C(m_{\rm p} \sin i, P)$ of the sample which corresponds, for a given couple $(m_{\rm p} \sin i, P)$, to the fraction of stars in the sample for which a companion with this mass and period is excluded by the detection limits (Borgniet et al. 2017). For the computation of the completeness we excluded HD 113337, for which companions were detected during the survey. The 40 to 90% search completeness values are presented in Fig. 21. We also computed the sample search completeness function C_D in this period and mass ranges (see Table 3). It is over 75% for the AF and FK sub-samples.

4.5. Companion occurrence rates

From our combined HARPS and SOPHIE sample of 119 stars, we computed the occurrence rates of GPs (1 to 13 $M_{\rm Jup}$) and BDs

[10] Assuming a circular orbit in the computation of the detection limits is common in the field of large RV surveys (Cumming et al. 2008; Lagrange et al. 2009; Borgniet et al. 2017; Grandjean et al. 2020) despite the slight underestimation of the detection limits it implies for the whole survey.

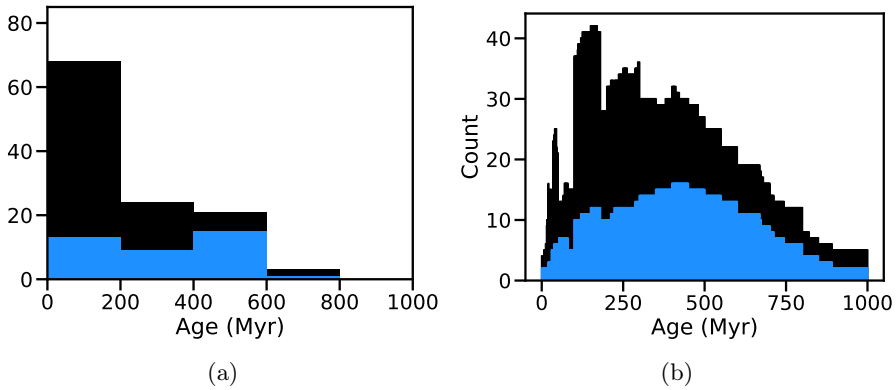

Fig. 15. Age distribution of the combined HARPS and SOPHIE YNS sample. (*a*) Age histogram. (*b*) Histogram of the possible age. Each bin counts the number of stars for which the bin is within their age error bars. The HARPS (black) histogram and the SOPHIE (blue) histogram are stacked.

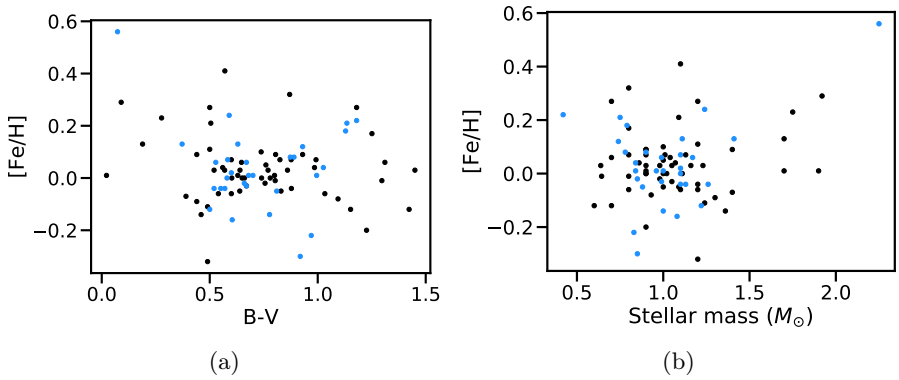

Fig. 16. Metallicity of the HARPS and SOPHIE YNS sample against $B-V$ (*a*) and against stellar mass (*b*). HARPS targets related data are in black and SOPHIE related data are in blue.

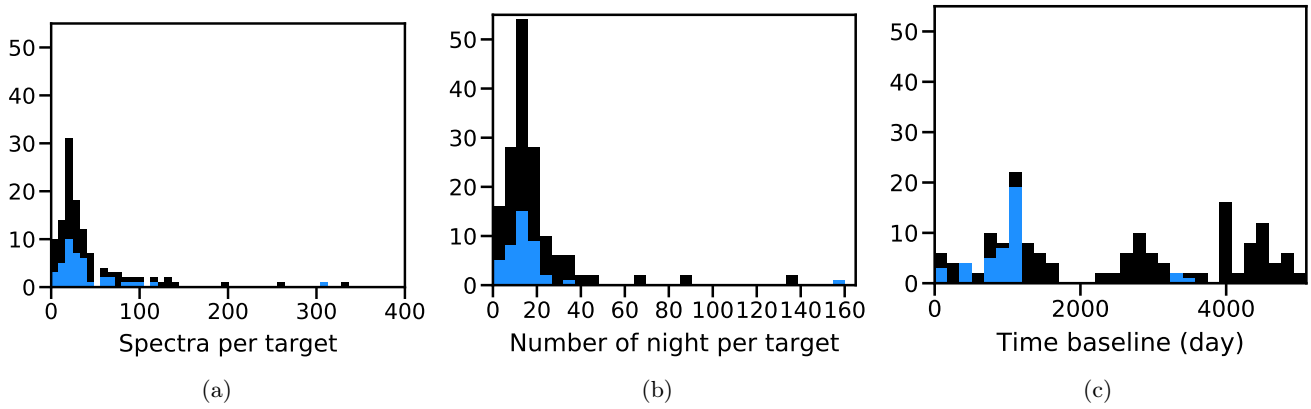

Fig. 17. Observation summary of the combined HARPS and SOPHIE YNS sample. (*a*) Histogram of the number of spectra per target; HD 216956 (Fomalhaut, 834 spectra) and HD 039060 (β Pic, 5108 spectra) are not displayed. (*b*) Histogram of the number of nights per target. (*c*) Histogram of the time baselines. The HARPS (black) histogram and the SOPHIE (blue) histogram are stacked.

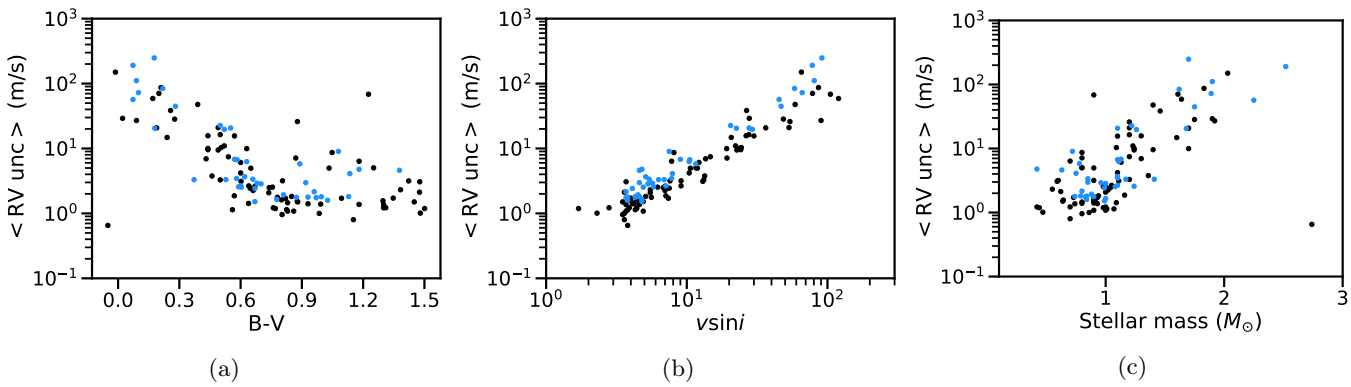

Fig. 18. Summary of the RV uncertainties of the combined survey. Mean RV uncertainty (accounting for the photon noise only) versus $B-V$(*a*), versus $v \sin i$ (*b*) and versus $M_\star$ (in $M_\odot$, c). HARPS targets related data are presented in black and SOPHIE related data are presented in blue.

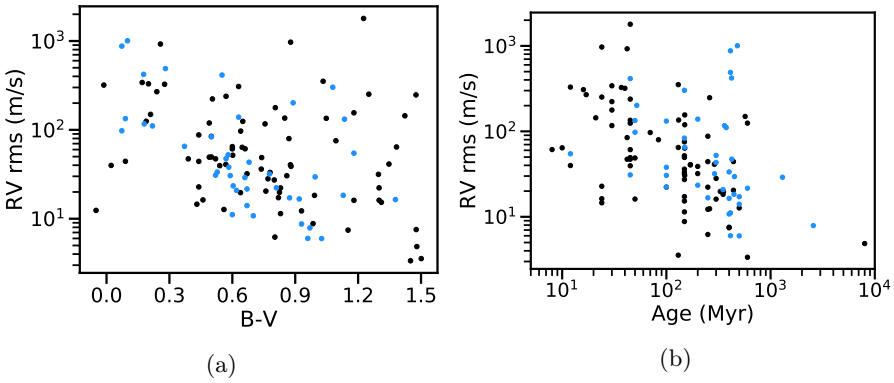

Fig. 19. Summary of the RV rms of the combined survey. RV rms versus $B-V$ (a), and versus age (b). HARPS targets related data are presented in black and SOPHIE related data are presented in blue.

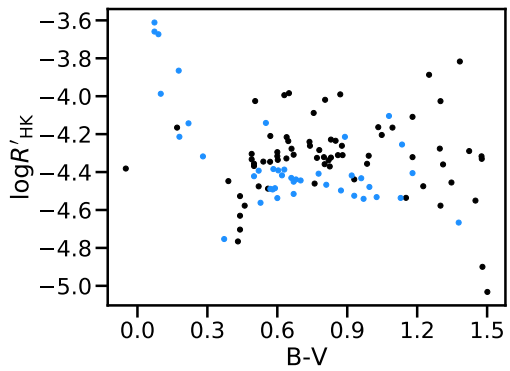

Fig. 20. Combined survey $\langle \log R'_{HK} \rangle$ versus $B-V$. The data from HARPS targets are shown in black and from SOPHIE targets in blue.

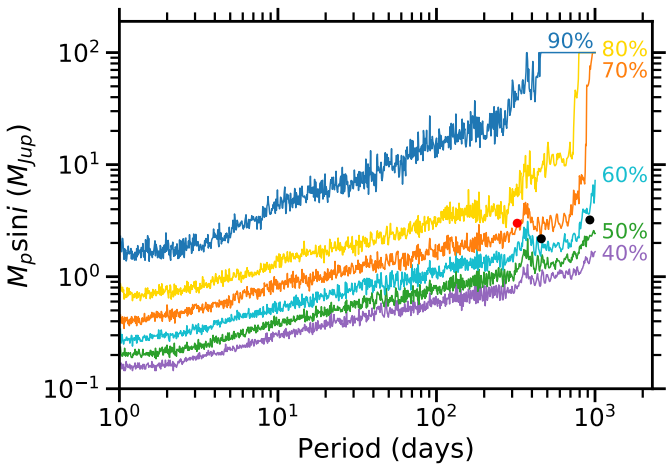

Fig. 21. Search completeness of our survey, corresponding to the lower $m_p \sin i$ for which X% of the stars in the survey have detection limits below this $m_p \sin i$ at a given period P; from bottom to top: 40% to 90%. Our detected planet HD 113337 b is shown as a red dot, while the non-detected planets in the survey, HD 128311 b and c, are shown as black dots.

(13 to 80 M_{Jup}) around AF-type ($B-V \in [-0.05 : 0.52[$), FK-type ($B-V \in [0.52 : 1.33[$), and KM-type ($B-V \geq 1.33$) stars, and for different ranges of periods: 1–10, 10–100, 100–1000, and 1–1000 days. We used the method described in Borgniet et al. (2017) to compute the occurrence rates and to correct them from the estimated number of missed companions n_{miss} derived from the search completeness. For the range where no companions were detected in the survey, only the upper limits of the occurrence rates are available.

The inclusion of the SOPHIE YNS survey targets in the combined sample provided a better constraint on the GP and BD occurrence rates around young stars in comparison to our previous study based on the HARPS YNS survey alone (Grandjean et al. 2020). As an example, the upper limits on the GP and BD occurrence rates are now 10 to 40% (depending on the period and mass range) lower than our previous estimate. Moreover, one GP system with $P < 1000$ days companions was discovered in the SOPHIE YNS survey, which permit us to derive the occurrence rates of these objects in this period range instead of an upper limit. We computed an occurrence rate of $1^{+2.2}_{-0.3}$% for GP with periods under 1000 days. The BD occurrence rate is below $0.9^{+2}_{-0.9}$% in this period range. We present these occurrence rates for AF, FK, M, and all stars in Table 3, and we present the AF and FK sub-samples occurrences rates in Fig. 22.

4.6. Comparison to surveys on main sequence stars

In our survey two companions with periods between 100 and 1000 days were detected on the same stars belonging to our AF sub-sample (HD 113337 b and c; Borgniet et al. 2014, 2019). However, we may have missed some planets with low masses and long periods as only 40% of the stars in the survey have detection limits lower than 2 M_{Jup} between 100 and 1000 days (see Fig. 21).

No HJ was detected in the survey. This non-detection is robust as 70% of our stars present limits of detection lower than 1 M_{Jup} for period lower than 10 days. In consequence only upper limits on the occurrence rates of HJ can be computed. To compare our results to previous surveys we adopted the same p-value formalism as in Grandjean et al. (2020). If the p-value of our non-detection of HJ around young stars is below 10% for a given occurrence rate on MS stars found in the literature, it indicates that the occurrence rate might be different between young and MS stars with a confidence level of 90%.

For the AF stars we computed an occurrence rate of $4.3^{+9.0}_{-1.3}$% for GP with periods lower 1000 days, which is in agreement with the $3.7^{+2.8}_{-1.1}$% occurrence rate derived by Borgniet et al. (2019) on all age AF MS stars. For the FK stars we computed an upper limit on the occurrence rate of $1.4^{+3.1}_{-1.4}$% for GP with periods lower 1000 days. It is compatible at 1σ with the GP occurrence rate of 4.3 ± 1% obtained by Cumming et al. (2008) on FK MS stars in the same period range, but it may be lower. The p-value test is validated with a confidence level of 90% ($p_{value} = 3^{+4}_{-2}$%), which indicates that the occurrence rates of these objects might be different between young and old FK stars. However, the level of confidence of this test is not strict, and the probability of observing such a difference is still about 10%. Moreover, it is puzzling that we do not observe a similar lack of close GPs around young

Table 3. GP ($m_p \sin i \in [1, 13]\ M_{Jup}$) and BD ($m_p \sin i \in [13, 80]\ M_{Jup}$) occurrence rates around young nearby stars computed from our combined HARPS and SOPHIE sample.

$m_p \sin i$ interval (M_{Jup})	Orbital period interval (day)	$B-V$	Search completeness C_D (%)	Detected GP systems	Missed GP systems upper limit	GP occurrence rate (%)	Confidence intervals 1σ (%)	Confidence intervals 2σ (%)
1–13	1–10	All	95	0	0.1	<0.9	0–2.9	0–4.9
(GP)		[−0.05 : 0.52[	**87**	**0**	**0.2**	**<3.7**	**0–11.5**	**0–19.1**
		[0.52 : 1.33[	*97*	*0*	*0.0*	*<1.3*	*0–4.2*	*0–7.1*
		≥1.33	***99***	***0***	***0.0***	***<11.2***	***0–29.7***	***0–45.6***
1–13	1–100	All	91	0	0.1	<0.9	0–3.0	0–5.1
		[−0.05 : 0.52[	**81**	**0**	**0.2**	**<4.0**	**0–12.4**	**0–20.5**
		[0.52 : 1.33[	*95*	*0*	*0.1*	*<1.3*	*0–4.3*	*0–7.3*
		≥1.33	***97***	***0***	***0.0***	***<11.5***	***0–30.4***	***0–46.6***
1–13	1–1000	All	87	1	0.2	1.0	0.7–3.1	0.2–5.4
		[−0.05 : 0.52[	**75**	**1**	**0.3**	**4.3**	**3.0–13.4**	**1.0–22.1**
		[0.52 : 1.33[	*91*	*0*	*0.1*	*<1.4*	*0–4.5*	*0–7.6*
		≥1.33	***89***	***0***	***0.1***	***<12.5***	***0–33.0***	***0–50.7***
13–80	1–10	all	99	0	0.0	<0.8	0–2.8	0–4.7
(BD)		[−0.05 : 0.52[	**98**	**0**	**0.0**	**<3.3**	**0–10.2**	**0–16.8**
		[0.52 : 1.33[	*97*	*0*	*0.0*	*<1.3*	*0–4.2*	*0–7.1*
		≥1.33	***100***	***0***	***0.0***	***<11.1***	***0–29.4***	***0–45.2***
13–80	1–100	All	97	0	0.0	<0.9	0–2.8	0–4.8
		[−0.05 : 0.52[	**97**	**0**	**0.0**	**<3.3**	**0–10.3**	**0–17.1**
		[0.52 : 1.33[	*98*	*0*	*0.0*	*<1.3*	*0–4.2*	*0–7.1*
		≥1.33	***100***	***0***	***0.0***	***<11.2***	***0–29.5***	***0–45.3***
13–80	1–1000	All	94	0	0.1	<0.9	0–2.9	0–4.9
		[−0.05 : 0.52[	**94**	**0**	**0.1**	**<3.4**	**0–10.6**	**0–17.5**
		[0.52 : 1.33[	*95*	*0*	*0.1*	*<1.3*	*0–4.3*	*0–7.3*
		≥1.33	***94***	***0***	***0.1***	***<11.8***	***0–31.4***	***0–48.1***

Notes. The parameters are displayed in normal, bold, italic, or bold italic fonts when considering the full star sample, the AF sub-sample, the FK sub-sample, or the M sub-sample, respectively.

AF stars, as our AF and FK sub-samples are not significantly different in metallicity and age. A statistical analysis on a larger number of FK young targets is needed to determine whether the GP occurrence rate is significantly lower for young FK stars than for MS FK stars.

Our upper limit on the occurrence rate of HJs ($P < 10$ days) around FK-type stars is $1.3^{+2.9}_{-1.3}$%, which is compatible with the HJ occurrence rate around FK MS stars estimated at $0.46^{+0.3}_{-0.3}$% by Cumming et al. (2008). We detected 0 companion out of 32 stars; the corresponding p-value is 86^{+9}_{-8}%.

We note that our upper limit on the GP occurrence rates around FK stars for periods lower than 1000 days is lower, but compatible at 1σ, with the occurrence rate we derived for AF stars on the same period range. If the occurrence rate of these planets is identical between AF and FK stars, then the p-value of our non-detection of such planets around our 32 AF stars will be 25^{+13}_{-24}%. The apparent difference in occurrence rates between young AF and FK stars is not likely to be significant, but a possibility that it is significant remains. The metallicity of our AF and FK sub-samples are not statically different. On the other hand, the stellar mass of these two sub-sample is significantly different. The occurrence rates of GP around young stars might then depend on the host star mass in favor of the high mass. This would be in agreement with the predictions of core accretion models (Kennedy & Kenyon 2008). It would also be in agreement with the host star mass-GP occurrence rate positive correlation observed for evolved stars in RV (Bowler et al. 2009; Johnson et al. 2010; Jones et al. 2016) and for wide orbit planets around young stars in direct imaging (Baron et al. 2019). A statistical analysis on larger and similarly sized young AF and FK samples is needed to determine whether the GP occurrence rate for FK young stars is significantly lower than for AF young stars.

Close BDs ($P < 1000$ days) are known to be rare (Grether & Lineweaver 2006; Sahlmann et al. 2011; Grieves et al. 2017; Jones et al. 2017; Borgniet et al. 2019). Our upper limit of $0.9^{+2}_{-0.9}$% on the BD occurrence rate for periods lower than 1000 days is consistent with the literature. A statistical analysis on a larger number of young targets is needed to study the difference in the BD occurrence rates between young and MS stars.

5. Conclusion

We carried out a 3-yr SOPHIE survey on 63 young A- to M-type stars in the search for close GP and BD companions. This survey allowed the discovery of a multiplanet system around HD 113337 (Borgniet et al. 2014, 2019); two binary companions, HD 112097 B and HD 105693 B; and a long-term trend on HD 109647. We confirmed numerous binary companions and we constrained for the first time the orbital parameters of HD 195943 B. No HJ or short-period ($P < 10$ days) BD was discovered in this survey.

We then combined our SOPHIE survey with the HARPS YNS survey that was presented in Grandjean et al. (2020), leading to a statistical analysis on 120 young stars. We obtained a GP occurrence rate of $0.9^{+2.2}_{-0.3}$% for periods lower than 1000 days and an upper limit on the BD occurrence rate of $0.9^{+2}_{-0.9}$% in the

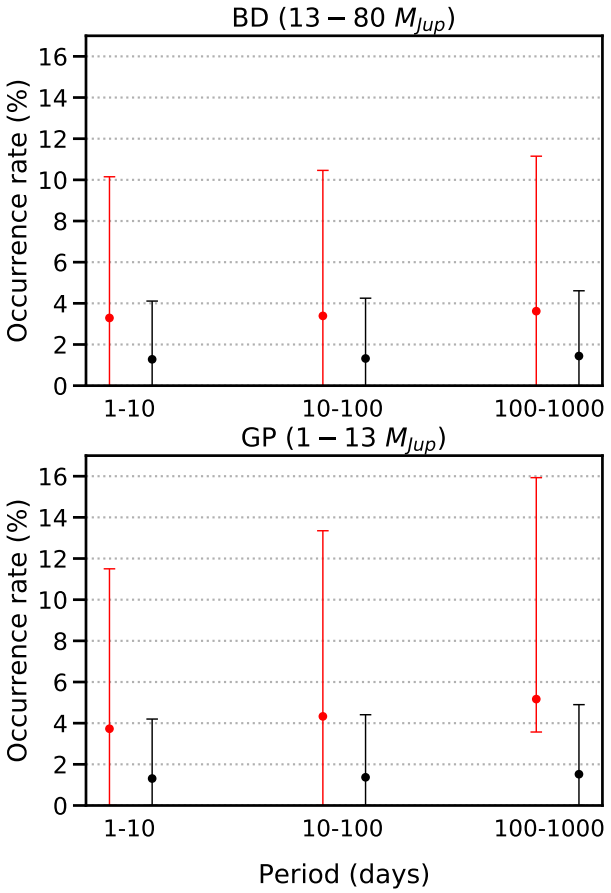

Fig. 22. Occurrence rates and their 1σ ranges for the period ranges of 1–10, 10–100, and 100–1000 days in the GP domain (1–13 $M_{\rm Jup}$, *top*) and BD domain (13–80 $M_{\rm Jup}$, *bottom*), for the AF sub-sample (red) and the FK sub-sample (black).

same period range. We observed a barely significant difference of close GP occurrence rate between AF-type and FK-type stars. We also observed a significant difference in GP occurrence rates between young and MS F- to K-type stars with a confidence level of 90%. An analysis of a larger number of young stars is needed to determine whether these differences are actually significant.

The forthcoming analysis of our HARPS survey on Sco-Cen stars will add 50 stars to our analysis. This will permit us to reduce the uncertainties on the derived occurrence rates for young stars, and will also help in the search for the possible impact of system ages on occurrence rates. Moreover, the Sco-Cen survey is mainly composed of early-type stars, which will balance our AF and FK sub-samples, allowing a better comparison of the two sub-sample occurrence rates.

Acknowledgements. We acknowledge support from the French CNRS and from the Agence Nationale de la Recherche (ANR grant GIPSE ANR-14-CE33-0018). This work has been supported by a grant from Labex OSUG@2020 (Investissements d'avenir – ANR10 LABX56). These results have made use of the SIMBAD database, operated at the CDS, Strasbourg, France. ESO SD acknowledges the support by INAF/Frontiera through the "Progetti Premiali" funding scheme of the Italian Ministry of Education, University, and Research. Based on observations collected at the European Southern Observatory under ESO programme(s) 060.A-9036(A), 072.C-0488(E), 072.C-0636(A), 072.C-0636(B), 073.C-0733(A), 073.C-0733(C), 073.C-0733(D), 073.C-0733(E), 074.C-0037(A), 074.C-0364(A), 075.C-0202(A), 075.C-0234(A), 075.C-0234(B), 075.C-0689(A), 075.C-0689(B), 076.C-0010(A), 076.C-0073(A), 076.C-0279(A), 076.C-0279(B), 076.C-0279(C), 077.C-0012(A), 077.C-0295(A), 077.C-0295(B), 077.C-0295(C), 077.C-0295(D), 078.C-0209(A), 078.C-0209(B), 078.C-0751(A), 078.C-0751(B), 079.C-0170(A), 079.C-0170(B), 079.C-0657(C), 080.C-0032(A), 080.C-0032(B), 080.C-0664(A), 080.C-0712(A), 081.C-0034(B), 081.C-0802(C), 082.C-0308(A), 082.C-0357(A), 082.C-0412(A), 082.C-0427(A), 082.C-0427(C), 082.C-0718(B), 083.C-0794(A), 083.C-0794(B), 083.C-0794(C), 083.C-0794(D), 084.C-1039(A), 085.C-0019(A), 087.C-0831(A), 089.C-0732(A), 089.C-0739(A), 090.C-0421(A), 091.C-0034(A), 094.C-0946(A), 098.C-0739(A), 099.C-0205(A), 0104.C-0418(A), 1101.C-0557(A), 183.C-0437(A), 183.C-0972(A), 184.C-0815(A), 184.C-0815(B), 184.C-0815(C), 184.C-0815(E), 184.C-0815(F), 191.C-0873(A), 192.C-0224(B), 192.C-0224(C), 192.C-0224(G), 192.C-0224(H). Based on observations collected at the Observatoire de Haute Provence under the programme(s) 06B.PNP.CONS, 07A.PNP.CONS, 07B.PNP.CONS, 08A.PNP.CONS, 13A.PNP.DELF, 13A.PNP.LAGR, 14A.PNP.LAGR.

References

Aguilera-Gómez, C., Ramírez, I., & Chanamé, J. 2018, A&A, 614, A55
Alsubai, K., Mislis, D., Tsvetanov, Z. I., et al. 2017, AJ, 153, 200
Ammler-von Eiff, M., & Guenther, E. W. 2009, A&A, 508, 677
Aumann, H. H. 1985, PASP, 97, 885
Backman, D. E., & Gillett, F. C. 1987, in Lecture Notes in Physics, 291, Cool Stars, Stellar Systems and the Sun, eds. J. L. Linsky, & R. E. Stencel (Berlin: Springer Verlag), 340
Baines, E. K., Armstrong, J. T., Schmitt, H. R., et al. 2018, AJ, 155, 30
Baron, F., Lafrenière, D., Artigau, É., et al. 2019, AJ, 158, 187
Beichman, C. A., Bryden, G., Stapelfeldt, K. R., et al. 2006a, ApJ, 652, 1674
Beichman, C. A., Tanner, A., Bryden, G., et al. 2006b, ApJ, 639, 1166
Bell, C. P. M., Mamajek, E. E., & Naylor, T. 2015, MNRAS, 454, 593
Bonavita, M., Desidera, S., Thalmann, C., et al. 2016, A&A, 593, A38
Booth, M., Kennedy, G., Sibthorpe, B., et al. 2013, MNRAS, 428, 1263
Bopp, B. W., & Fekel, F. C. 1975, PASP, 87, 891
Borgniet, S., Boisse, I., Lagrange, A. M., et al. 2014, A&A, 561, A65
Borgniet, S., Lagrange, A. M., Meunier, N., & Galland, F. 2017, A&A, 599, A57
Borgniet, S., Lagrange, A.-M., Meunier, N., et al. 2019, A&A, 621, A87
Bouchy, F., & Sophie Team. 2006, in Tenth Anniversary of 51 Peg-b: Status of and Prospects for Hot Jupiter Studies, eds. L. Arnold, F. Bouchy, & C. Moutou, 319
Bowler, B. P., Johnson, J. A., Marcy, G. W., et al. 2009, ApJ, 709, 396
Brandt, T. D., Kuzuhara, M., McElwain, M. W., et al. 2014, ApJ, 786, 1
Butler, R. P., Marcy, G. W., Vogt, S. S., et al. 2003, ApJ, 582, 455
Carleo, I., Benatti, S., Lanza, A. F., et al. 2018, A&A, 613, A50
Carpenter, J. M., Bouwman, J., Mamajek, E. E., et al. 2009, ApJS, 181, 197
Casagrande, L., Schönrich, R., Asplund, M., et al. 2011, A&A, 530, A138
Chauvin, G., Desidera, S., Lagrange, A.-M., et al. 2017a, in SF2A-2017: Proceedings of the Annual meeting of the French Society of Astronomy and Astrophysics, eds. C. Reylé, P. Di Matteo, F. Herpin, E. Lagadec, A. Lançon, Z. Meliani, & F. Royer, 331
Chauvin, G., Desidera, S., Lagrange, A.-M., et al. 2017b, A&A, 605, L9
Chavero, C., de la Reza, R., Ghezzi, L., et al. 2019, MNRAS, 487, 3162
Chen, C. H., Patten, B. M., Werner, M. W., et al. 2005, ApJ, 634, 1372
Chen, C. H., Mittal, T., Kuchner, M., et al. 2014, ApJS, 211, 25
Choquet, E., Perrin, M. D., Chen, C. H., et al. 2016, ApJ, 817, L2
Churcher, L., Wyatt, M., & Smith, R. 2011, MNRAS, 410, 2
Collier Cameron, A., Guenther, E., Smalley, B., et al. 2010, MNRAS, 407, 507
Corder, S., Carpenter, J. M., Sargent, A. I., et al. 2009, ApJ, 690, L65
Cotten, T. H., & Song, I. 2016, ApJS, 225, 15
Cox, A. N. 2000, Allen's Astrophys. Quant.
Cumming, A., Butler, R. P., Marcy, G. W., et al. 2008, PASP, 120, 531
da Silva, L., Girardi, L., Pasquini, L., et al. 2006, A&A, 458, 609
David, T. J., Petigura, E. A., Luger, R., et al. 2019, ApJ, 885, L12
de la Reza, R., & Pinzón, G. 2004, ApJ, 128, 1812
Deleuil, M., Bonomo, A. S., Ferraz-Mello, S., et al. 2012, A&A, 538, A145
Delorme, P., Lagrange, A. M., Chauvin, G., et al. 2012, A&A, 539, A72
Delorme, P., Schmidt, T., Bonnefoy, M., et al. 2017, A&A, 608, A79
Desidera, S., Covino, E., Messina, S., et al. 2015, A&A, 573, A126
Donaldson, J. K., Roberge, A., Chen, C. H., et al. 2012, ApJ, 753, 147
Donati, J. F., Moutou, C., Malo, L., et al. 2016, Nature, 534, 662
Durkan, S., Janson, M., & Carson, J. C. 2016, ApJ, 824, 58
Eiroa, C., Marshall, J. P., Mora, A., et al. 2013, A&A, 555, A11
Eisenbeiss, T., Ammler-von Eiff, M., Roell, T., et al. 2013, A&A, 556, A53
Escorza, A., Karinkuzhi, D., Jorissen, A., et al. 2019, A&A, 626, A128
Esposito, M., Guenther, E., Hatzes, A. P., & Hartmann, M. 2006, in Tenth Anniversary of 51 Peg-b: Status of and Prospects for Hot Jupiter Studies, eds. L. Arnold, F. Bouchy, & C. Moutou, 127
Fekel, F. C., Henry, G. W., & Tomkin, J. 2017, AJ, 154, 120
Fernandes, R. B., Mulders, G. D., Pascucci, I., Mordasini, C., & Emsenhuber, A. 2019, ApJ, 874, 81
Figueira, P., Marmier, M., Bonfils, X., et al. 2010, A&A, 513, L8

Fischer, D. A., & Valenti, J. 2005, ApJ, 622, 1102
Folsom, C. P., Bouvier, J., Petit, P., et al. 2018, MNRAS, 474, 4956
Frankowski, A., Jancart, S., & Jorissen, A. 2007, A&A, 464, 377
Fuhrmann, K., Chini, R., Kaderhandt, L., & Chen, Z. 2017, ApJ, 836, 139
Gagné, J., Plavchan, P., Gao, P., et al. 2016, ApJ, 822, 40
Gaia Collaboration (Brown, A. G. A., et al.) 2018, A&A, 616, A1
Galicher, R., Marois, C., Macintosh, B., et al. 2016, A&A, 594, A63
Galland, F., Lagrange, A. M., Udry, S., et al. 2005a, A&A, 444, L21
Galland, F., Lagrange, A. M., Udry, S., et al. 2005b, A&A, 443, 337
Gallet, F., & Bouvier, J. 2015, A&A, 577, A98
Gáspár, A., Rieke, G. H., & Ballering, N. 2016a, ApJ, 826, 171
Gáspár, A., Rieke, G. H., & Ballering, N. 2016b, ApJ, 826, 171
Golimowski, D. A., Krist, J. E., Stapelfeldt, K. R., et al. 2011, ApJ, 142, 30
Grandjean, A., Lagrange, A. M., Beust, H., et al. 2019, A&A, 627, L9
Grandjean, A., Lagrange, A. M., Keppler, M., et al. 2020, A&A, 633, A44
Grether, D., & Lineweaver, C. H. 2006, ApJ, 640, 1051
Grieves, N., Ge, J., Thomas, N., et al. 2017, MNRAS, 467, 4264
Han, I., & Gatewood, G. 2002, PASP, 114, 224
Hartmann, M., & Hatzes, A. P. 2015, A&A, 582, A84
Hernán-Obispo, M., Gálvez-Ortiz, M. C., Anglada-Escudé, G., et al. 2010, A&A, 512, A45
Hernán-Obispo, M., Tuomi, M., Gálvez-Ortiz, M. C., et al. 2015, A&A, 576, A66
Hillenbrand, L. A., Carpenter, J. M., Kim, J. S., et al. 2008, ApJ, 677, 630
Hines, D. C., Schneider, G., Hollenbach, D., et al. 2007, ApJ, 671, L165
Holland, W. S., Greaves, J. S., Zuckerman, B., et al. 1998, Nature, 392, 788
Huélamo, N., Figueira, P., Bonfils, X., et al. 2008, A&A, 489, L9
Jackman, J. A. G., Wheatley, P. J., Bayliss, D., et al. 2019, MNRAS, 489, 5146
Johns-Krull, C. M., McLane, J. N., Prato, L., et al. 2016, ApJ, 826, 206
Johnson, J. A., Aller, K. M., Howard, A. W., & Crepp, J. R. 2010, PASP, 122, 905
Jones, M. I., Jenkins, J. S., Brahm, R., et al. 2016, A&A, 590, A38
Jones, M. I., Brahm, R., Wittenmyer, R. A., et al. 2017, A&A, 602, A58
Kalas, P., Liu, M. C., & Matthews, B. C. 2004, Science, 303, 1990
Kalas, P. G., Rajan, A., Wang, J. J., et al. 2015, ApJ, 814, 32
Kennedy, G. M., & Kenyon, S. J. 2008, ApJ, 673, 502
Kiraga, M. 2012, Acta Astron., 62, 67
Kley, W., & Nelson, R. P. 2012, ARA&A, 50, 211
Koen, C., & Eyer, L. 2002, MNRAS, 331, 45
Koenig, B., Fuhrmann, K., Neuhaeuser, R., Charbonneau, D., & Jayawardhana, R. 2002, in Astronomische Gesellschaft Abstract Series, 19, Astronomische Gesellschaft Abstract Series, 17
Kovári, Z., Strassmeier, K., Granzer, T., et al. 2004, A&A, 417, 1047
Lagrange, A. M., Desort, M., Galland, F., Udry, S., & Mayor, M. 2009, A&A, 495, 335
Lagrange, A.-M., Meunier, N., Chauvin, G., et al. 2013, A&A, 559, A83
Lagrange, A. M., Meunier, N., Rubini, P., et al. 2019, Nat. Astron., 421
Lang, K. R. 1999, Astrophys. Formulae (Springer: New York)
Lannier, J., Delorme, P., Lagrange, A. M., et al. 2016, A&A, 596, A83
Lawler, S. M., Beichman, C. A., Bryden, G., et al. 2009, ApJ, 705, 89
Lépine, S., & Bongiorno, B. 2007, AJ, 133, 889
Lindgren, S., & Heiter, U. 2017, A&A, 604, A97
Lippincott, S. L., & Worth, M. D. 1978, PASP, 90, 330
Luck, R. E. 2017, AJ, 153, 21
Luck, R. E. 2018, AJ, 155, 111
Makarov, V. V., & Kaplan, G. H. 2005, AJ, 129, 2420
Mamajek, E. E. 2012, ApJ, 754, L20
Mamajek, E. E., Meyer, M. R., Hinz, P. M., et al. 2004, ApJ, 612, 496
Mann, A. W., Newton, E. R., Rizzuto, A. C., et al. 2016, AJ, 152, 61
Mannings, V., & Barlow, M. J. 1998, ApJ, 497, 330
Matthews, B. C., Sibthorpe, B., Kennedy, G., et al. 2010, A&A, 518, L135
Mayor, M., Pepe, F., Queloz, D., et al. 2003, The Messenger, 114, 2
McArthur, B. E., Benedict, G. F., Henry, G. W., et al. 2014, ApJ, 795, 41
McDonald, I., Zijlstra, A. A., & Boyer, M. L. 2012, MNRAS, 427, 343
Melo, C., Santos, N. C., Gieren, W., et al. 2007, A&A, 467, 721
Meshkat, T., Bailey, V., Rameau, J., et al. 2013, ApJ, 775, L40
Messina, S., Desidera, S., Turatto, M., Lanzafame, A. C., & Guinan, E. F. 2010, A&A, 520, A15
Messina, S., Millward, M., Buccino, A., et al. 2017, A&A, 600, A83
Metchev, S. A. 2006, PhD Thesis, California Institute of Technology, California, USA
Meunier, N., Lagrange, A. M., & De Bondt, K. 2012, A&A, 545, A87
Meyer, M. R., Hillenbrand, L. A., Backman, D. E., et al. 2004, ApJS, 154, 422
Meyer, M. R., Carpenter, J. M., Mamajek, E. E., et al. 2008, ApJ, 673, L181
Milli, J., Hibon, P., Christiaens, V., et al. 2017, A&A, 597, L2
Montesinos, B., Eiroa, C., Mora, A., & Merín, B. 2009, A&A, 495, 901
Montet, B. T., Crepp, J. R., Johnson, J. A., Howard, A. W., & Marcy, G. W. 2014, ApJ, 781, 28
Moór, A., Ábrahám, P., Kóspál, A., et al. 2013, ApJ, 775, L51
Morales, F. Y., Bryden, G., Werner, M. W., & Stapelfeldt, K. R. 2016, ApJ, 831, 97
Morin, J., Donati, J. F., Petit, P., et al. 2008, MNRAS, 390, 567
Moro-Martín, A., Marshall, J. P., Kennedy, G., et al. 2015, ApJ, 801, 143
Muller, P. 1950, J. Observ., 33, 105
Newton, E. R., Irwin, J., Charbonneau, D., et al. 2017, ApJ, 834, 85
Nidever, D. L., Marcy, G. W., Butler, R. P., Fischer, D. A., & Vogt, S. S. 2002, ApJS, 141, 503
Nielsen, E. L., De Rosa, R. J., Rameau, J., et al. 2017, AJ, 154, 218
Nordström, B., Mayor, M., Andersen, J., et al. 2004, A&A, 418, 989
Olmedo, M., Chávez, M., Bertone, E., & De la Luz, V. 2013, PASP, 125, 1436
Olspert, N., Lehtinen, J. J., Käpylä, M. J., Pelt, J., & Grigorievskiy, A. 2018, A&A, 619, A6
Passegger, V. M., Reiners, A., Jeffers, S. V., et al. 2018, A&A, 615, A6
Patel, R. I., Metchev, S. A., & Heinze, A. 2014, ApJS, 212, 10
Patel, S. G., Vogt, S. S., Marcy, G. W., et al. 2007, ApJ, 665, 744
Paulson, D. B., & Yelda, S. 2006, PASP, 118, 706
Pecaut, M. J., Mamajek, E. E., & Bubar, E. J. 2012, ApJ, 746, 154
Perrier, C., Sivan, J. P., Naef, D., et al. 2003, A&A, 410, 1039
Perruchot, S., Bouchy, F., Chazelas, B., et al. 2011, in Society of Photo-Optical Instrumentation Engineers (SPIE) Conference Series, 8151, Techniques and Instrumentation for Detection of Exoplanets V, ed. S. Shaklan, 815115
Plavchan, P., Werner, M. W., Chen, C. H., et al. 2009, ApJ, 698, 1068
Pollack, J. B., Hubickyj, O., Bodenheimer, P., et al. 1996, Icarus, 124, 62
Poveda, A., Allen, C., Costero, R., Echevarría, J., & Hernández-Alcántara, A. 2009, ApJ, 706, 343
Rameau, J., Chauvin, G., Lagrange, A.-M., et al. 2013a, ApJ, 772, L15
Rameau, J., Chauvin, G., Lagrange, A. M., et al. 2013b, A&A, 553, A60
Rebull, L. M., Stapelfeldt, K. R., Werner, M. W., et al. 2008, ApJ, 681, 1484
Rebull, L. M., Stauffer, J. R., Bouvier, J., et al. 2016, ApJ, 152, 114
Rhee, J. H., Song, I., Zuckerman, B., & McElwain, M. 2007, ApJ, 660, 1556
Rizzuto, A. C., Newton, E. R., Mann, A. W., et al. 2020, AJ, 160, 33
Rutten, R. G. M. 1986, A&A, 159, 291
Saffe, C., & Gómez, M. 2004, A&A, 423, 221
Sahlmann, J., Ségransan, D., Queloz, D., et al. 2011, A&A, 525, A95
Santos, N. C., Israelian, G., Mayor, M., et al. 2005, A&A, 437, 1127
Schneider, G., Silverstone, M. D., Hines, D. C., et al. 2006, ApJ, 650, 414
Ségransan, D., Mayor, M., Udry, S., et al. 2011, A&A, 535, A54
Sierchio, J. M., Rieke, G. H., Su, K. Y. L., & Gáspár, A. 2014, ApJ, 785, 33
Simon, M., & Schaefer, G. H. 2011, ApJ, 743, 158
Smith, B. A., & Terrile, R. J. 1984, Science, 226, 1421
Smith, R., Wyatt, M. C., & Haniff, C. A. 2012, MNRAS, 422, 2560
Soto, M. G., Jenkins, J. S., & Jones, M. I. 2015, MNRAS, 451, 3131
Soummer, R., Perrin, M. D., Pueyo, L., et al. 2014, ApJ, 786, L23
Stauffer, J., Rebull, L., Bouvier, J., et al. 2016, AJ, 152, 115
Stencel, R. E., & Backman, D. E. 1991, ApJS, 75, 905
Stone, J. M., Skemer, A. J., Hinz, P. M., et al. 2018, AJ, 156, 286
Strassmeier, K. G., Pichler, T., Weber, M., & Granzer, T. 2003, A&A, 411, 595
Su, K. Y. L., Rieke, G. H., Stapelfeldt, K. R., et al. 2009, ApJ, 705, 314
Su, K. Y., Bryden, G., Rieke, G., Stapelfeldt, K. R., & Balog, Z. 2013, in American Astronomical Society Meeting Abstracts, 221, 144.19
Teyssandier, J., Lai, D., & Vick, M. 2019, MNRAS, 486, 2265
Tokovinin, A. 2014a, AJ, 147, 86
Tokovinin, A. 2014b, ApJ, 147, 87
Tremko, J., Bakos, G. A., Žižňovský, J., & Pribulla, T. 2010, Contrib. Astron. Observ. Skalnate Pleso, 40, 83
van Eyken, J. C., Ciardi, D. R., von Braun, K., et al. 2012, ApJ, 755, 42
van Leeuwen, F. 2007, A&A, 474, 653
Vigan, A., Bonavita, M., Biller, B., et al. 2017, A&A, 603, A3
Vogt, S. S., Butler, R. P., Marcy, G. W., et al. 2005, ApJ, 632, 638
Weise, P., Launhardt, R., Setiawan, J., & Henning, T. 2010, A&A, 517, A88
Wilson, P. A., Hébrard, G., Santos, N. C., et al. 2016, A&A, 588, A144
Wittenmyer, R. A., Endl, M., Cochran, W. D., Levison, H. F., & Henry, G. W. 2009, ApJS, 182, 97
Wright, N. J., Drake, J. J., Mamajek, E. E., & Henry, G. W. 2011, ApJ, 743, 48
Wright, J. T., Marcy, G. W., Howard, A. W., et al. 2012, ApJ, 753, 160
Yu, L., Donati, J.-F., Hébrard, E. M., et al. 2017, MNRAS, 467, 1342
Zorec, J., & Royer, F. 2012, A&A, 537, A120
Zuckerman, B., & Song, I. 2004, ApJ, 603, 738
Zuckerman, B., Rhee, J. H., Song, I., & Bessell, M. S. 2011, ApJ, 732, 61
Zuckerman, B., Vican, L., Song, I., & Schneider, A. 2013, ApJ, 778, 5

Appendix A: Combined sample

The tables are available at the CDS.

Appendix B: Age and mass estimations

When available, the ages and masses of the targets of the HARPS YNS and the SOPHIE YNS surveys were taken from the literature. When it was possible, the ages and masses were derived using the methods described in Desidera et al. (2015) and in an upcoming paper, then on a homogeneous scale with the above works. Briefly, we considered membership to groups and associations (adopting the group ages from Bonavita et al. (2016), also discussed in the upcoming paper); indirect indicators such as rotation, chromospheric, and coronal activity; and Li 6708 Å equivalent width, complemented by isochrone fitting. Preference was given to the moving group criterion whenever possible (confirmed members). For field objects the weight assigned to the various methods depends on color and/or spectral type and age range (e.g., saturation of chromospheric activity and coronal emission versus age below 100–150 Myr, and high sensitivity of lithium to age for K dwarfs younger than 300–500 Myr, with limits only at older ages). Masses were derived using the PARAM interpolation code[11] (da Silva et al. 2006), as in Desidera et al. (2015). For the remaining targets the masses were estimated from the spectral type by using an empirical $M_* = f$(B-V) relation (see page 564 of Lang 1999 and p. 209 of Cox 2000).

[11] http://stev.oapd.inaf.it/cgi-bin/param_1.3